SINGLE MOLECULE FLUORESCENCE STUDIES OF RIBOSOME DYNAMICS: AN APPLICATION OF METAL ENHANCED FLUORESCENCE

DISSERTATION

Presented to the Graduate Council of the

Graduate School of Biomedical Science

University of North Texas

Health Science Center at Fort Worth

in Partial Fulfillment of the Requirements

For the Degree of

Doctor of Philosophy

By

Shashank Bharill, M.S

Fort Worth, Texas

May 2010

ACKNOWLEDGEMENTS

Unusual but fortunate, my PhD saw more mentors than total number of lab members due to the huge number of collaborations of my advisor Dr. Zygmunt Gryczynski. First and foremost, I offer my sincere gratitude to three of many supervisors I had, Dr. Zygmunt Gryczynski, Dr. Ignacy Gryczynski and Dr. Yale Goldman. It would not have been easy to finish this degree without Dr. Gryczynskis not only because of their guidance and patience but also the much needed entertainment throughout my work in the lab but nothing comes one way in this world. They probably still wonder why milk bars (krufkas) in their office get over so soon and why at times their coffee suddenly turns so sweet or salty. One simply could not wish for a friendlier environment than they provided.

I was really fortunate to work in Dr. Yale Goldman's lab at University of Pennsylvania for a significant period of my PhD. I attribute the most important part of my degree to his encouragement, effort and advice. He is really a knowledgeable mentor and sometimes I wonder how he finds time to manage such diverse projects in Physics, Engineering, Biophysics, Electronics, and Biology. I enjoyed every bit of my time in his lab excluding those exceptional extended Thursday meetings (2-7 pm). I am also grateful to the other lab members in Dr. Yale and Dr. Gryczynski labs (CCFT) for their valuable discussions in and out of the lab.

With good lab, one also needs to have a good PhD committee. I feel really lucky to have such a great committee led by Dr. Robert Luedtke with Dr. Julian Borejdo, Dr. Raghu Krishnamoorthy and Dr. Porunelloor Mathew as the committee members. I have always seen students from my

department and others struggle in their grant writing course due to the misconception of it being an exam and wondered if I would ever be able to deal with it. It was this wise committee, especially Dr. Robert Luedtke, who taught me the essence of the course. I owe the distinction I was awarded for the 6010 to their excellent guidance. I really want to thank all of them for being such great teachers.

I would especially like to thank two postdoctoral associates, Dr. Chunlai Chen in Yale's lab and Dr. Rafal Luchowski in Gryczynski lab. I want to thank Chunlai who helped me with my data analysis using Matlab due to my meager knowledge in programming and also helped me in many other ways during my stay. I also want to thank Rafal for his help with single molecule experiments, though most of them did not work but we often compensated the frustration with our unprecedented late night extended coffee meetings, occasionally joined by Pabak. It would be unfair to forget post doc Baba (rechristened) for providing us ample opportunities to laugh even at tough times.

It is inadequate to say that my friends supported me. I would not have been able to do my work with the required zeal without them. I have no words to thank Ribha and Gitanjali who supported and encouraged me (from thousands of miles away, in India) when I moved to Dr. Goldman's lab and had a hard time initially in a new city. Thank you for being my friends and for the love and persistent confidence in me. I cannot forget my apartment-mates, Dilip and Aniket with whom I shared most of my evenings cooking delicious Indian dishes for them and next day hearing in school that Aniket is an awesome cook, thanks mates! I realize now how many people have contributed to my degree and many of them go unnoticed here but not in my heart.

Finally, I thank my parents and family in India for supporting me throughout all my studies. Without them, their love and inspiration, I would not be where I am today.

TABLE OF CONTENTS

LIST OF ILLUSTRATIONS

Chapter I

LIST OF TABLES

Chapter IV

LIST OF ABBREVIATIONS

AFM	Atomic Force Microscopy
ALEX	Alternating Laser EXcitation
APD	Avalanche Photodiode
EM-CCD	Electron Multiplying Charge Coupled Device
FCS	Fluorescence Correlation Spectroscopy
FRET	Fluorescence Resonance Energy Transfer
ICs	Initiation Complexes
MEF	Metal Enhanced Fluorescence
QD	Quantum Dots
SD	Shine-Dalgarno
SmFRET	Single molecule FRET
SMF	Single Molecule Fluorescence
TIRF	Total Internal Reflection Fluorescence

CHAPTER I

INTRODUCTION TO THE STUDY

Over the past two decades, fluorescence technology has become a valuable tool in biomedical research. It is a dominant technology expanding to different branches of biology; for example, biotechnology, genetic analysis, medical diagnosis, etc. This enormous rate of expansion is primarily due to its high sensitivity and ease of handling. This has also led to its extensive use in molecular and cellular imaging that is very useful in determining numerous cellular processes including localization of intracellular molecules even at the single molecule level.

The Fluorescence Phenomenon: Fluorescence is a type of luminescence where a fluorophore absorbs light (excitation) at specific wavelength (corresponding to the transition energy barrier) and emits longer wavelength light. This emission of light occurs from electronically excited singlet states of the molecule. In the singlet state, spin vectors are completely antiparallel and thus the total spin S=0. Electron excited from the singlet ground state yield only the singlet excited state which decays quickly back to the ground state yielding fluorescence (Fig 1) (1, 2). This phenomenon leads to the rapid rate of emission in fluorescence that is typically in the range of nanoseconds. Occasionally, however, singlet excited state can get converted into a triplet state after excitation. In triplet state, the decay back to the ground state is slow (milli seconds to seconds) and this light yielding process is known as phospohorescence (Fig 1) (1, 2). This can be easily explained using Jablonski diagram. Jablonski diagram is often used in many forms to illustrate various molecular processes that occur during absorption and emission. In this diagram,

S_0, S_1, S_2 and S_3 represent singlet ground, and first, second and third excited singlet states, respectively (bold black lines).

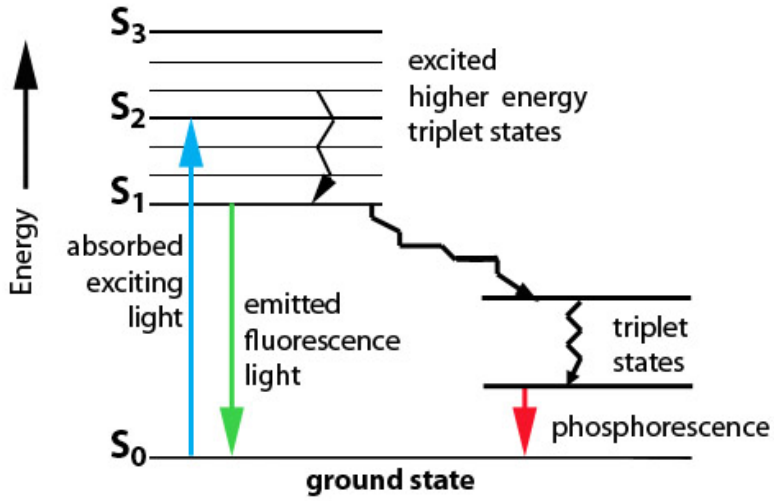

Fig 1. Basic Jablonski Diagram (modified from Principles of Fluorescence Spectroscopy, third edition)

At each of these electronic states, electron can stay in any of the vibrational level depicted by light black lines. Upon absorption of light by a fluorophore, electron of the molecule transits mostly from lowest vibrational level of the ground state and is excited to other vibrational level of excited states, S_1, S_2 or S_3. From this vibrational level of excited states, electron then relaxes back to the lowest vibrational level of the S_1 excited state. This is known as Internal Conversion and occurs in time less than 10^{-12} Sec, which is certainly before emission, which is in the range of nanoseconds. From this lowest vibrational level of excited state S_1, electron then finally relaxes to some vibrational level of the ground state, S_0, resulting in fluorescence emission. Return of the electron to higher vibrational level of the ground state S_0 causes vibrational structures in the emission of some fluorophores whereas others are smooth due to the return of electron into the lowest vibrational level of S_0 (1, 2).

In some cases, electron can also undergo a spin conversion to the first triplet state, T_1. This is known as Intersystem crossing. Electron from T_1, moves then to S_0 but at a very slow rate since it is forbidden and this type of delayed emission is known as Phosphorescence (Fig 1) (1, 2).

Generally, the energy of emission is lower than that of absorption. In other words, emission wavelength is generally longer than the absorption wavelength. This effect is known as Stokes Shift. One of the main reasons for Stokes Shift is internal conversion in which electron loses some of its energy. In addition to internal conversion, energy loss can also occur by thermalization of extra vibrational energy (where electron relaxes to higher vibrational levels first and then relaxes to the lowest), solvent effects, excited-state reactions, complex formation and energy transfer (Fig 2).

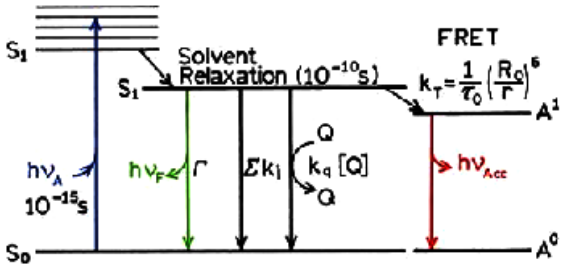

Fig 2. Jablonski Diagram with collisional quenching and FRET (from Principles of Fluorescence Spectroscopy, third edition)

Quantum Yield and Lifetimes: As discussed above, transition from S_1 to S_0 occurs with loss of some energy. As a result, the number of photons emitted by a fluorophore is rarely equal to the

number of photons absorbed by it. This ratio of emitted photons to absorbed photons is known as Quantum yield (1) and can be calculated by:

$$Q = \frac{\Gamma}{\Gamma+\kappa_{nr}}$$

Where Γ is the radiative decay rate and $K_{n\,r}$ is the non-radiative decay

Before relaxing back to the ground state, the average time that the molecule spends in the excited state after absorption of a photon is known as its lifetime (1, 2). It is given by:

$$\tau = \frac{1}{\Gamma+\kappa_{nr}}$$

Where Γ is the radiative decay rate and $K_{n\ r}$ is the non-radiative decay

If the quantum yield of the fluorophore is 1 then lifetime of the fluorophore is known as natural lifetime and is given by:

$$\tau_n = \frac{1}{\Gamma}$$

Where Γ is the radiative decay rate.

Fluorescence Techniques: In the past several years, advances in fluorescence technology led to its innovative uses in various forms. These fluorescence techniques are now widely used in determining various cellular processes. Some of the widely used fluorescence techniques are described below:

(I) Fluorescence Anisotropy: Fluorescence anisotropy measures the rotational diffusion of a molecule using the polarized fluorescence signal from the molecule. Anisotropy measurements are typically used to measure binding interaction between molecules; for example, protein-

protein interactions (3), protein-DNA interactions (4) etc. It also calculates the binding constant of these interactions. In addition, it also provides the information regarding molecular size and shape of the molecules.

The basic idea of anisotropy measurements is photoselective excitation of fluorophores by polarized light. Those molecules having absorption transitions aligned parallel to the electric vector of the photons have the highest possibility of excitation (Fig 3) (1). This distribution of molecules excited by vertically polarized light is given by:

$$f(\theta)\mathrm{d}\theta = \cos^2\theta \sin \mathrm{d}\theta$$

Where θ is the angle that absorption dipole makes with Z-axis

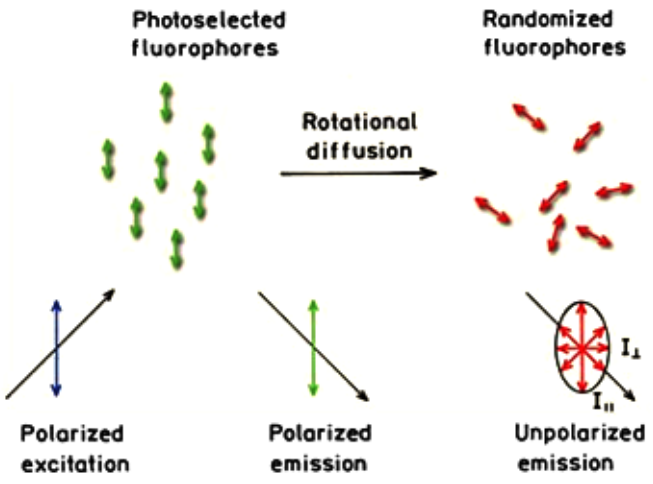

Fig 3. Effects of polarized excitation and rotational diffusion on the anisotropy of the emission (from Principles of Fluorescence Spectroscopy, third edition)

Hence, upon excitation of molecules with polarized light, only selective fluorophores get excited and this results in partially polarized emission from the excited fluorophores (1). Anisotropy can be determined by:

$$r = \frac{I_{\parallel} - I_{\perp}}{I_{\parallel} + 2I_{\perp}}$$

Where $I_{\parallel}$ and $I_{\perp}$ are vertical and horizontal intensities, respectively.

As expected, if there is rotational diffusion between the time of absorption and emission, then the anisotropy will decrease and finally reach to zero if the diffusion is very fast (1). Hence, measurement of rotational diffusion is important in determining the relative angular displacement of the flurophore between absorption and emission. If rotational diffusion is the only process leading to loss of anisotropy, then anisotropy can be determined by Perrin equation

$$r = \frac{r_0}{1 + (\tau/\theta)}$$

Where r_0 is the measured anisotropy in absence of any rotational diffusion and θ is the correlation time for the rotational diffusion.

Therefore, fluorescence anisotropy is sensitive to the rate of rotational diffusion and is useful in measuring binding interaction between molecules since rotational diffusion decreases upon binding interactions.

(II) Fluorescence Correlation Spectroscopy: Fluorescence correlation spectroscopy (FCS) is a widely used technique to characterize the dynamics of fluorescent molecules. It is useful in determining processes like protein - protein interactions and membrane processes like endo and

exocytosis that are difficult to determine with other fluorescence techniques (5, 6). It is based on determining the fluorescence intensity fluctuations in a very small observed volume over time. These intensity fluctuations are bursts of photons from single fluorophores diffusing in and out of the observed volume. It requires concentration (pico to nano molar) of fluorophores at the single molecule level since higher concentrations can generate smaller fluctuations and also cause averaging of the signal (5, 6).

FCS also gets affected if the solution is too viscous since it will retain the molecules in the observed volume for a longer time and there will be less intensity fluctuations (1, 5, 6). In addition, molecules will be more prone to bleaching which can make calculations more complicated. Intensity fluctuations (amplitude and speed) in the observed volume is basically used to determine the correlation function (temporal correlation). This autocorrelation function, normalized by average intensity squared, is given by

$$G'(\tau) = \frac{<F(\tau)F(t+\tau)>}{<F><F>}$$

Where F(t) is fluorescence intensity at time t, F(t+τ) is fluorescence intensity after a delay time τ

The height and position of correlation curve on time axis (Fig 4C) determines the average number of fluorophores and their diffusion coefficient.

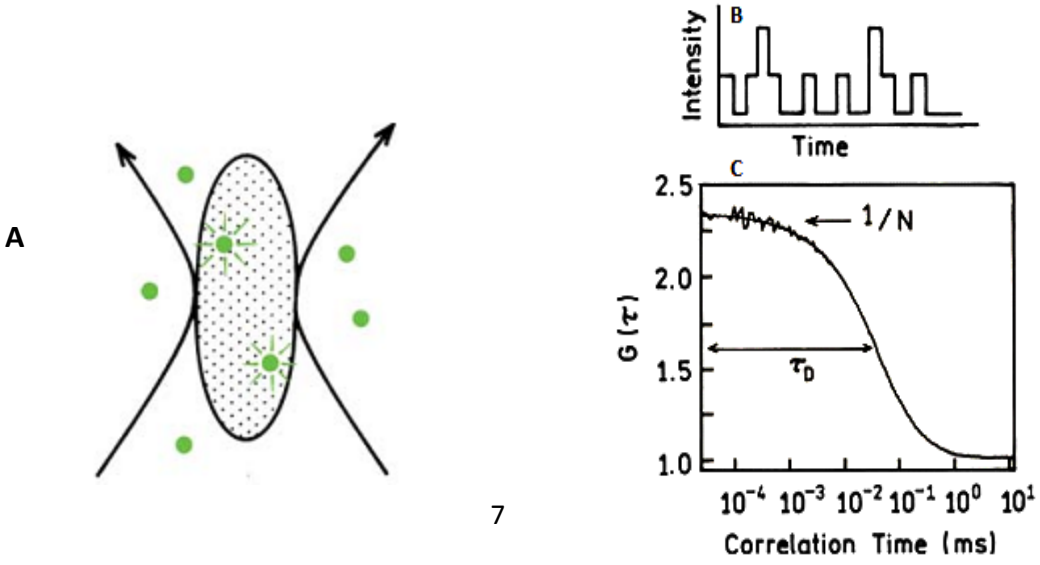

Fig 4. Fluorescence correlation spectroscopy, A. Observed volume B. Intensity fluctuations and C. Correlation function (from Principles of Fluorescence Spectroscopy, third edition)

Fluorescence Resonance Energy Transfer: Fluorescence Resonance Energy Transfer (FRET) is an excited state process that occurs when emission spectra of one fluorophore (donor) overlaps with absorption spectra of another fluorophore (acceptor) (Fig 5) (1). This can be used in determining the interaction between two molecules and to obtain an idea of distance between them (7). This is very useful in determining various *in vitro* and *in vivo* cellular processes (8). In FRET, donor does not fluoresce in order to transfer its energy to the acceptor; rather it is the resonance between the two that transfers the energy from the donor to the acceptor (1). The donor and acceptor remains coupled by a dipole-dipole interaction. The extent of FRET is determined primarily by two factors

(i) Distance between donor and acceptor molecule

(ii) Spectral overlap between emission of donor and absorption of acceptor (R_0)

R_0 is the distance at which there is 50% energy transfer between donor and acceptor.

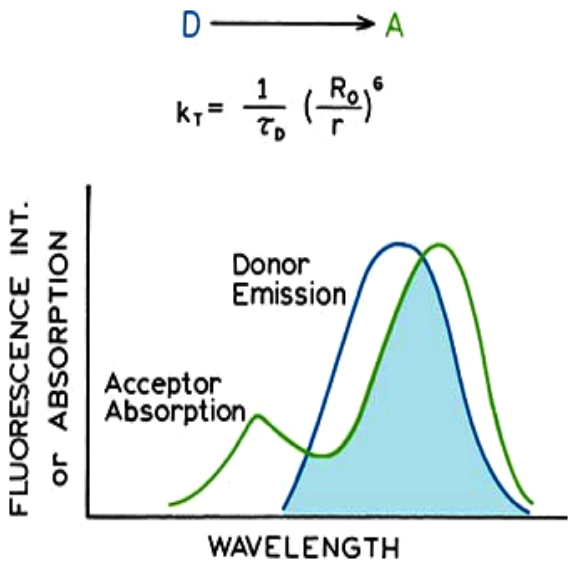

Fig 5. Spectral overlap for fluorescence resonance energy transfer (FRET) (from Principles of Fluorescence Spectroscopy, third edition)

Efficiency of energy transfer (E) is calculated by intensity/lifetime of donor molecule in presence and absence of acceptor molecule (1, 7, 8)

$$E = 1 - \frac{F_{DA}}{F_D}$$

or

$$E = 1 - \frac{\tau_{DA}}{\tau_D}$$

F_{DA} & F_D and τ_{DA} & τ_D are the fluorescence intensities and lifetimes, respectively, of donor in presence and absence of acceptor

The energy transfer efficiency can then be used to calculate the distance between donor and acceptor since it is required when interaction between the molecules is sought. It can be calculated by (1, 7, 8)

$$r = R_0 \sqrt[6]{\frac{1}{E} - 1}$$

Where R_0 is the Forster distance and E is the efficiency of energy transfer

Finally, rate of energy transfer is calculated by (1, 7, 8)

$$k_T(r) = \frac{1}{\tau_D} \left(\frac{R_0}{r}\right)^6$$

Where τ_D is the donor lifetime in absence of acceptor, R_0 is the Forster distance and r is the actual distance between donor and acceptor

Since this rate is added as a non-radiative decay rate, both Quantum yield and lifetime of the donor gets affected (1, 7, 8). Modified Jablonski diagram is depicted in Fig 2. This is an ensemble FRET where large numbers of donor and acceptor molecules are present in the reaction mixture and hence react randomly. FRET calculations become more complicated when one donor interacts with more than one acceptor or vice versa. To overcome this and other averaging effects, single molecule FRET (smFRET) has been developed in the past decade.

FRET at Single Molecule Level (smFRET): Single molecule FRET has gained much attention in the past decade. This is done to avoid the averaging effect of the ensemble reaction and is much more precise (9-14). Using smFRET, several important biological problems have been solved with precision at the single molecule level without complicated effects of averaging. Most important requirement in SMD is to immobilize the molecules on the glass surface; for example, donor molecule and then flow in the acceptor molecules. Donor only or both donor and acceptor molecules are then excited using donor laser or both donor acceptor lasers. When both the lasers have to be used, they are not used at the same time but used alternatively for a short period of time. This type of excitation is known as Alternating Laser EXcitation (ALEX) (15). After excitation, emission from single donor acceptor molecules can be collected as single molecule trajectories (Fig 6) by imaging the immobilized molecules in total internal reflection (TIRF) mode using either charge coupled device (CCD camera) or avalanche photodiode (APD) detectors (14).

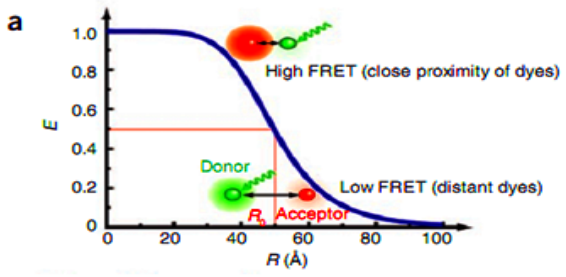

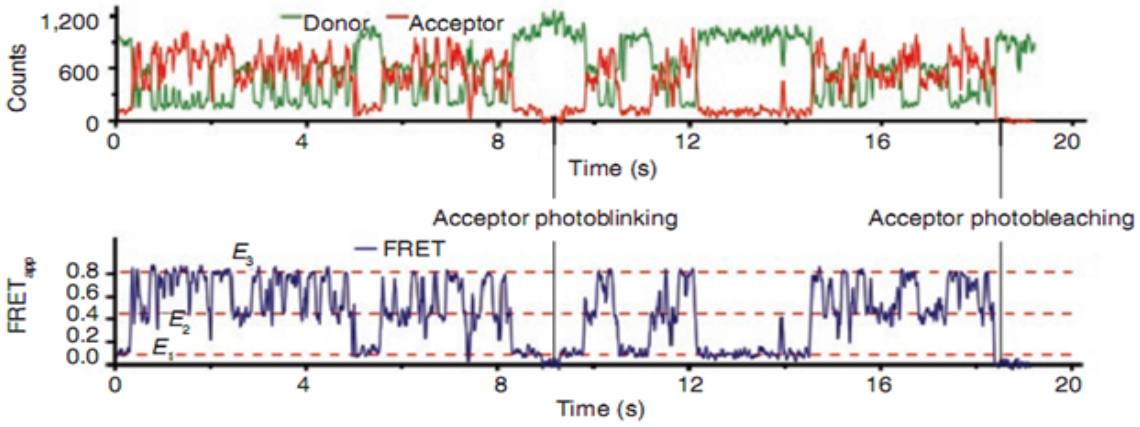

Fig 6. SmFRET description, A. FRET efficiency E as a function of inter-dye distance (R) for a R_0 = 50 Å. At R = R_0, E = 0.5, but at smaller distance, E >0.5 and vice versa. B. Two color FRET data, upper panel: donor acceptor intensities, bottom: Apparent FRET efficiency calculated from donor-acceptor intensities above (from Roy, R et al, Nature Methods, June 2008)

Special confocal optics is required for this process of single molecule FRET or detection. A schematic is shown below for smFRET spectroscopy using TIRF based microscopy (Fig 7) (14).

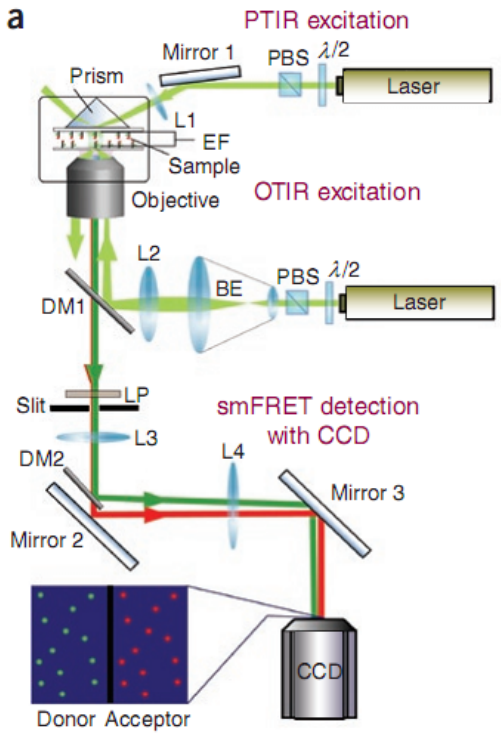

Fig 7. Schematic of smFRET spectroscopy. A. TIR excitation and single FRET emission detection. Tethered single molecules either excited by PTIR or OTIR. Fluorescence is collected using objective. The collimated image is split into donor and acceptor emissions and imaged side by side on CCD camera (from Roy, R et al, Nature Methods, June 2008).

From the recorded intensity traces of donor and acceptor molecules, average intensities from all donors and acceptor molecules are calculated and apparent FRET efficiency is calculated by (14)

$$E_{app} = I_A/(I_A + I_D)$$

Where I_D and I_A are donor and acceptor intensity, respectively with donor excitation

Actual FRET efficiency is then calculated by determining the crosstalk and background in both the channels, and differences in quantum yield and detection efficiency between the donor and acceptor molecules. Actual FRET efficiency is then given by (14)

$$E = \left[1 + \frac{I_D}{I_A - \chi I_D}\,\gamma\right]^{-1}$$

Where I_D and I_A are donor and acceptor intensity, respectively with donor excitation. X is cross talk of donor into acceptor channel and γ accounts for the difference in quantum yield and detection efficiency between donor and acceptor molecules.

γ factor can be calculated by

$$\gamma = \Delta I_A / \Delta I_D$$

Where ΔI_A and ΔI_D are change in acceptor and donor fluorescence intensities upon acceptor photobleaching and change in FRET value.

Very important factor while performing smFRET is photostability of donor and acceptor molecules. Since higher laser powers are used in smFRET, in order to acquire enough number of photons from single donor and acceptor molecules, dyes tend to photobleach faster (16, 17). In order to improve photostability, both selections of dyes and enzymatic oxygen-scavenging system (glucose oxidase, catalase and β-D glucose) with triplet state quencher Trolox is important. Oxygen scavenging system sequesters oxygen in the reaction mixture and prevents its reaction with fluorophores in their excited states and trolox quenches the triplet state formation in the fluorophore; thus preventing photobleaching and photoblinking respectively. Quantum dots are preferable in certain cases since they are very photostable compared to other organic dyes but their irregular photoblinking is a big concern in smFRET (18). Metal surfaces have also been in use since last decade as they improve photostability of fluorophores by reducing the lifetime of the fluorophore and increasing the rate of electron relaxation from excited to ground state (19).

Metal Enhanced Fluorescence: As discussed above, single molecule detection needs higher laser powers to collect enough number of photons which causes rapid photobleaching of the dyes due to low intensity and poor photostability of the organic dyes (16, 17). In addition to this they also show strong photoblinking effect. Therefore, there is the need for brighter photo stable dyes

with minimum blinking to improve single molecule studies. Quantum dots were thought to be an alternative since they are very bright and photostable. However, because of their strong photoblinking, they cannot be used in single molecule studies especially smFRET (18). Utilizing the surface plasmons of noble metals to engineer the spectral properties of the fluorophores and enhance their fluorescence is another approach that could be used to improve the fluorescence intensity, photostability and photoblinking (19). This alteration in the properties of a fluorophore, in presence of metal particles, occurs mainly due to two phenomenons. First is the presence of localized enhanced electromagnetic field and second is radiative decay engineering due to the presence of metallic particles (20-22). Localized enhanced electromagnetic field results in strong excitation of the fluorophores. Radiative decay engineering of the fluorophores occurs due to the coupling interaction of the excited fluorophore with the nearby metal particles where fluorophore act as an oscillating dipole causing resonance with metallic electrons (20-22). This interaction increases the radiative rate of the fluorescence due to unknown mechanism and makes the fluorophore brighter. This phenomenon is defined as metal enhance fluorescence (MEF). If the fluorophores are very close (>5nm) to the metal particles, then it results in the quenching of fluorescence (Fig 8).

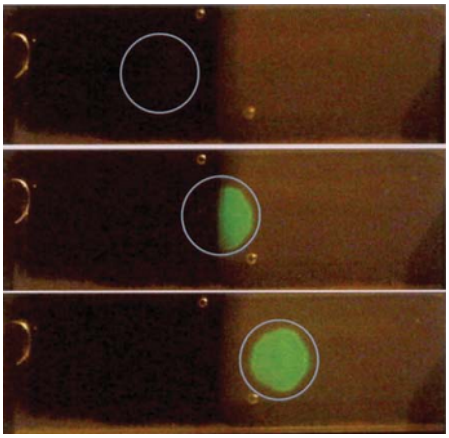

Fig 8. Effect of metallic silver particles on surface bound fluorescein labeled human serum albumin. Left, no silver and right with silver particles (from Principles of Fluorescence Spectroscopy, third edition)

In addition to increased fluorescence emission, this metal-fluorophore interaction also causes a number of beneficial effects, such as increase in quantum yield and decrease in lifetime (1). Decrease in lifetime in turn causes increase in photostability since fluorophores have to stay in the excited state for a shorter period of time and hence less probability of getting photobleached (Fig 9) (23, 24).

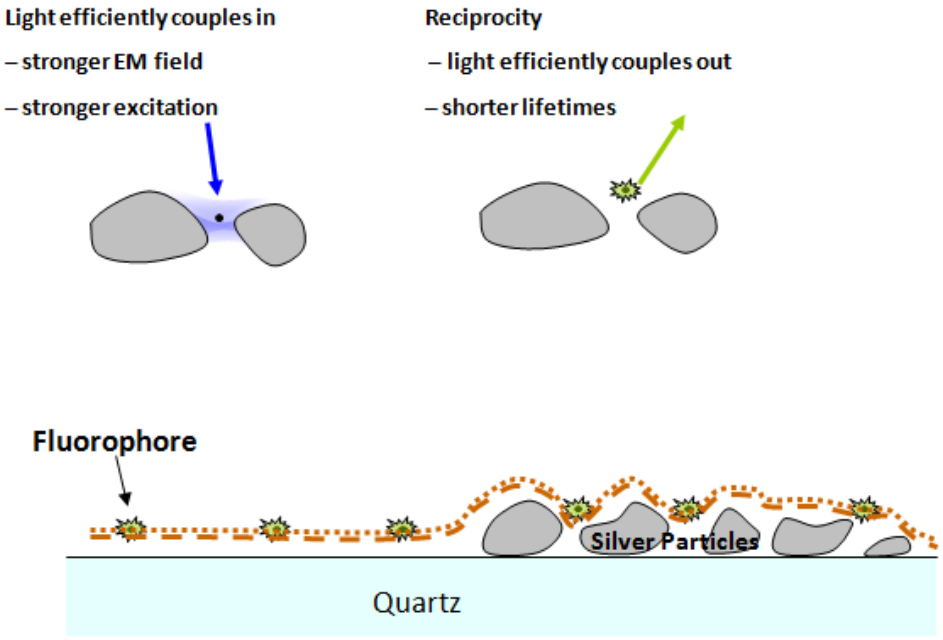

Fig 9. Schematic of effects of silver particles on fluorophores (from Principles of Fluorescence Spectroscopy, second edition)

Since radiative rate of the fluorophore gets altered by the metal-fluorophore interaction, quantum yield and lifetime also gets affected and is now given by (1)

$$Q_m = \frac{\Gamma + \Gamma_m}{\Gamma + \Gamma_m + \kappa_{nr}}$$

$$\tau_m = (\Gamma + \Gamma_m + \kappa_{nr})^{-1}$$

Γ is the radiative rate and Γ_m is increase in radiative rate due to the metal particles. K_{nr} is the non-radiative decay rate.

Jablonski diagram will now show an extra radiative rate decay component (Γ_m) and an extra excitation component (Em) due to metal particles (Fig 10) (1)

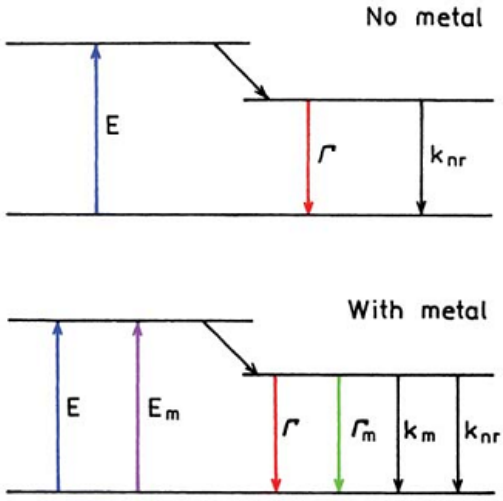

Fig 10. Jablonski diagram without (top) and with (bottom) the effects of near metal particles. E_m is additional excitation in presence of metal particles (from Principles of Fluorescence Spectroscopy, third edition)

Biological Model: We have used protein synthesis machinery in our study. This machinery involves a lot of molecules; messenger RNA (mRNA), transfer RNA (tRNA), ribosomes with initiation and elongation factors. First three molecules are explained in details below whereas the initiation factors and elongation factors have been explained in brief later.

Messenger RNA (mRNA): Messenger RNAs are single stranded molecules that are synthesized by transcription of genomic DNA by RNA polymerases (25, 26). They have special features to attach with ribosomes and get decoded into the proteins, the functional product of central dogma. Eukaryotic mRNA molecules are monocistronic, with a few exceptions, but prokaryotic mRNA molecules are mostly polycistronic so as to save resources and energy and lengthen their lifespan.

Polycistronic mRNAs are single mRNA molecules that can synthesize more than one protein. Unlike alternate splicing, where single mRNA is shuffled to get relatively different proteins, polycistronic mRNA molecules contain different messages, for different proteins, transcribed together. A well known example of polycistronic mRNA is Lac operon mRNA of E.Coli. Lac operon polycistronic mRNA is 5300 ribonucleotides long and contains message for 3 different proteins, B-Galactosidase (z), Permease (y) and Acetylase (a) (25). Messenger RNA molecules have precise points of start and stop and all messages in polycistronic mRNA have these start and stop signals for each of its message. Start signal usually has a purine rich sequence that is complimentary to pyrimidine rich sequence of 16s RNA of ribosome (Fig 11) known as Shine Dalgarno (SD) sequence (25, 26).

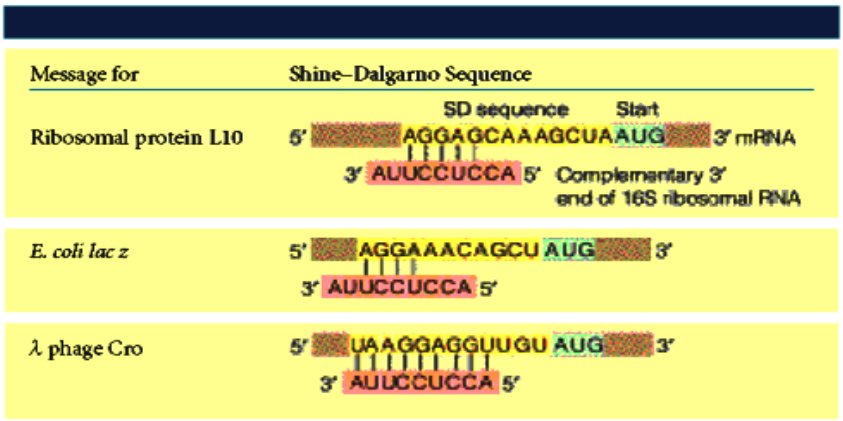

Fig 11. Shine Dalgarno sequences and their complementary sequence on 16S ribosomal RNA (from Biochemistry by Mathews, third edition).

This sequence helps mRNA to get aligned into the ribosome enabling the ribosome to start synthesizing protein from the correct site of mRNA efficiently. This sequence provides a level of regulation of gene expression since minor difference in the sequence results in increase or

decrease in gene expression; for example, B-Galactosidase gets translated more than permease and acetylase due to differences in their SD sequences (Fig 12) (25, 26). Some mRNA molecules also regulate the gene expression by having secondary/tertiary structures at their 5' ends and thus either does not get translated efficiently or change the rate of their degradation by mRNA degrading enzymes like AUF 1 (27).

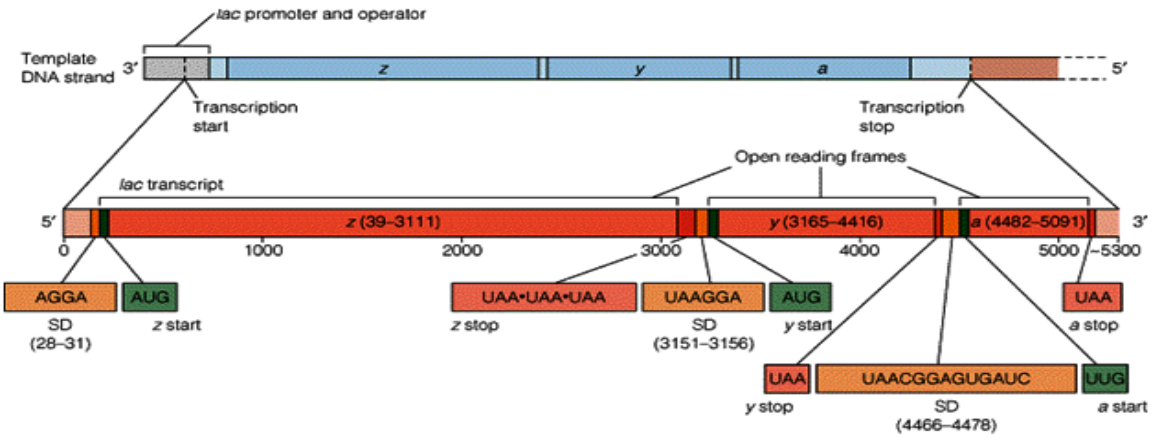

Fig 12. The lac operon gene and its transcript. Each gene in this polycistronic mRNA is flanked by start, stop and SD sequence (from Biochemistry by Mathews, third edition).

Transfer RNA (tRNA): Transfer RNA molecules serve as the adaptor, a molecule that holds amino acid at its one end (3' end) and recognizes anticodon by its other end (anticodon loop) and helps in decoding of the mRNA message. First tRNA molecule to be sequenced was tRNA alanine from yeast by Robert Holley in 1965. All tRNA molecules are folded in cloverleaf pattern and have similar structural pattern. This is because all of them have to interact with ribosomes, mRNAs and elongation factors in a similar way in order to reduce the number of molecules they interact (25, 26). For, example, if they have different structures then they all need

different enzymes to charge them. Also, they all would not be able to fit A, P and E sites of the same ribosomes and that makes protein synthesis impossible. All tRNA molecules thus have common structural features cited below (25, 26):

(i) All tRNA molecules are of similar size (~25 Kd) and contain between 73-96 ribonucleotides.

(ii) They also contain bases other than A, U, G and C. For example, they all have inosine, pseudouridine, dihydrouridine, ribothymidine, and methylated and phosphorylated forms of bases.

(iii) These modifications are performed by certain enzymes and are very important in maintaining tertiary structure of tRNA molecules. For example, all these modified bases are found at unstructured part of the tRNA molecules, which means they prevent the formation of unnecessary structures and deformity. Methylation, for example, provides the hydrophobic character to certain parts of the tRNAs that are important in their interaction with ribosomes and synthetases.

(iv) The 5’ terminal of all the tRNA molecules is phoshorylated and the 3’ is hydroxylated. The 3’ end has conserved sequence of CCA.

(v) Anticodon is always flanked by 2 pyrimidines at 5’end and by one modified purine and other variable base at 3’ end (Py-Py-Anticodon-Modified Purine-X).

(vi) They are L-shaped molecules; usually having two segments of double helix. These helical segments are perpendicular to each other thus providing the L-shape to the molecule (Fig 13).

(vii) To stabilize the molecules, most of the non helical bases form unusual hydrogen bonding interactions, with the help of their 2'OH, that are not complimentary (GG, AA etc). Moreover, base stacking plays a major role in providing stability to these structures (Fig 14).

(viii) In contrast, some part of the molecules do not have strong interactions with each other (for ex: CCA terminus and adjacent helical region). This is to provide flexibility to that part of the molecule so that it can fit easily in the active site of synthetases and E, P, and A site of the ribosomes.

(ix) Amino acid binding site and anticodon loop are at the opposite end of the tRNA molecules, approximately (~80 Å) apart.

(x) Multiple tRNA molecules are synthesized as a single long RNA precursor and then cleaved by ribonucleases (Fig 15).

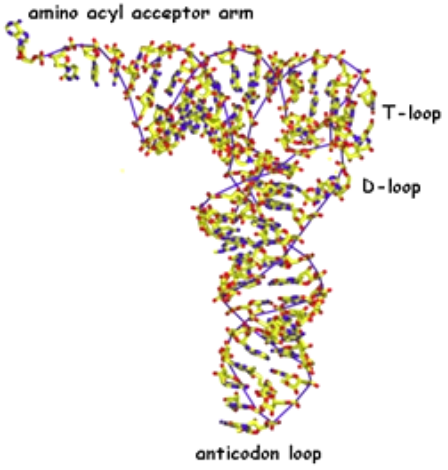

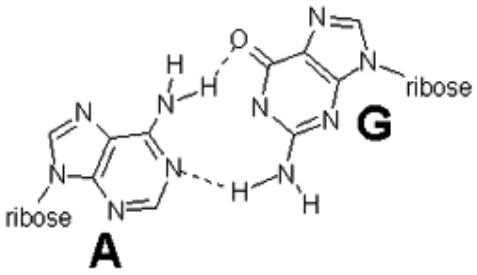

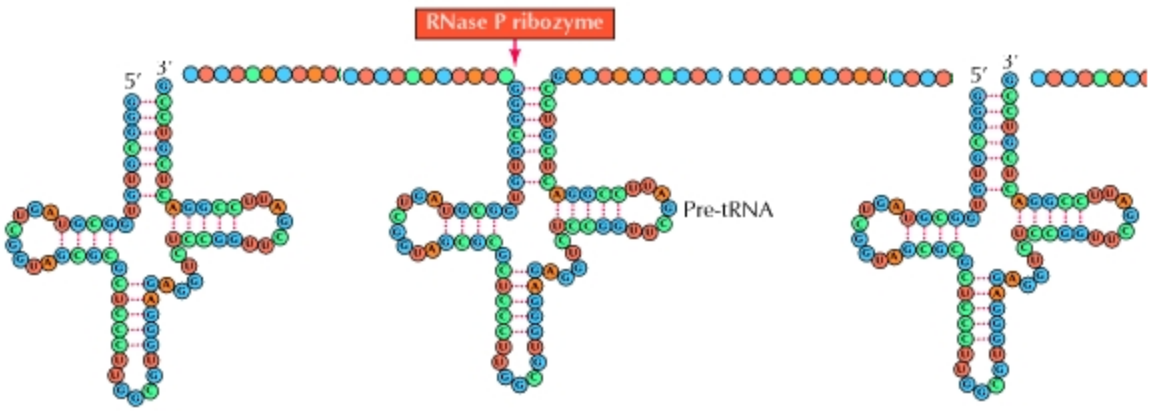

Fig 13. L- shaped structure of tRNA showing helical segments, Fig 14. Non-complimentary base pairing between two purines (A and G), and Fig 15. Precursor molecule of multiple tRNA molecules showing cleavage site of ribozyme.

Ribosomes: In protein synthesis, a series of codons on mRNA direct the synthesis of the protein chain. In addition to the two molecules of machinery described above (mRNA and tRNA), this process involves another molecule, ribosome, on which this process takes place. Ribosome manages the movement of tRNA and mRNA with high speed and accuracy that is much needed for this process. Ribosomes are complicated ribonucleoprotein molecules made up of 2 subunits (25, 26). These subunits are 30S and 50S in bacteria that associate to form 70S; 50S subunit contains 23S and 5S rRNA and 31 different proteins whereas 30S subunit has 16 S rRNA and 21 protein molecules (Fig 16) (25, 26). These RNA molecules form double helical structures that are supported by ribosomal proteins. These structures are highly conserved and even found to have compensatory mutations to maintain base pairing and correct folding (25). Both 30S and 50S subunits have 3 binding sites for tRNA molecules; A site (aminoacyl), P site (peptidyl) and E site (exit). A site is the site of entry for incoming aminoacylated tRNA molecules, P site holds the peptidyl tRNA and E site holds the deacylated tRNA molecules before they leave the ribosomes (25, 26). The 30S subunit holds both mRNA and tRNA molecules and monitor the

base pairing between codon and anticodon, providing fidelity to the process. The 50S subunit, on the other hand holds 3'end of the tRNA molecule and catalyzes peptide bond formation between the peptide chain on P site tRNA and newly entered amino acid in the A site (25, 26). Both 50S and 30S subunits then help in translocation of tRNA and mRNA precisely one codon at a time. This translocation also involves other protein factors, some of them are GTPases activated by the ribosome.

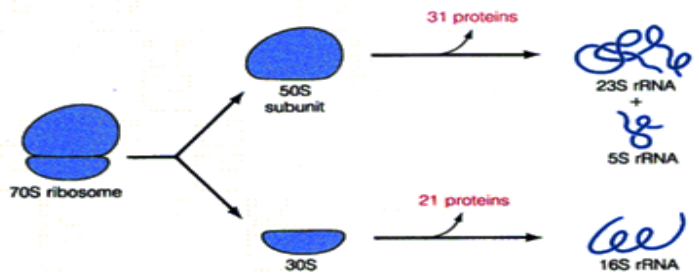

Fig 16. RNA and protein components of a 70S prokaryotic ribosome (from Biochemistry by Mathews, third edition).

This biological process has been determined in 1960's and 70's but due to the lack of sophisticated molecular tools, mechanistic details could not be determined. However, in the last two decades, rapid and qualitative progress has been made in the field due to the development of various approaches in different fields, for example; single molecule detection, single particle reconstruction techniques, combined with cryoelectron microscopy (cryo EM), crystallography, etc (28). Due to these developments and efforts, atomic structures of both subunits and 5.5 Å resolution molecular model of entire bacterial ribosome (Fig 17) has been determined (28a). For determining the entire ribosome structure with mRNA and tRNA molecules in addition to other factors, Drs Venkatraman Ramakrishnan, Thomas A. Steitz and Ada. E. Yonath, have been awarded Nobel Prize in Chemistry in 2009.

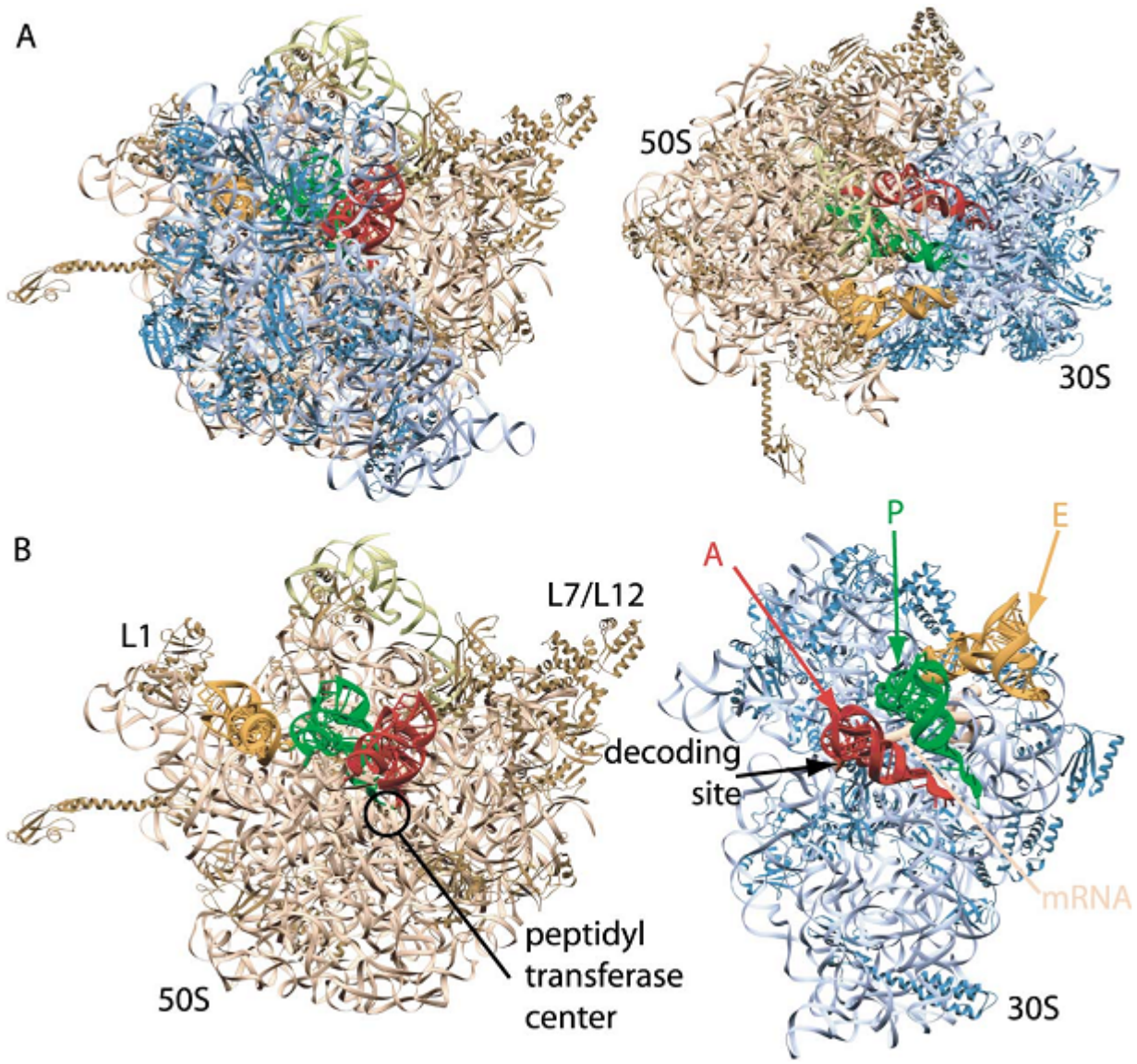

Fig 17. Crystal structure of ribosome, A shows two views of 70S ribosome complexed with mRNA and tRNA, B is exploded view of 50S and 30S subunits showing A, P and E site tRNA molecules (V Ramakrishnan, Cell, Feb 2002).

Crystal Structure: After many years of effort; the first high resolution 2.4 Å structure of 50S subunit from archaean *Holoarcula marismortuii* was determined in 2000 (29). This structure shows a very important feature of ribosome, peptidyl transferase center. But at this resolution,

several important structures such as L1 stalk, L11-RNA region and L7/L12 stalk appeared to be disordered. Despite these deformities, this structure is of importance since it shows water molecules, metal ions and base modifications with sufficient resolution, which are very crucial in understanding the stability and folding of ribosome and orientation of tRNA molecules in the ribosomes. In 2001, 3.1 Å resolution structure of 50S subunit from *Deinococcus radioduarans* had been reported (30). This structure was similar to the one from *Holoarcula* but also has some of the structures that were disordered in the previous structure. Two independent studies have determined the 30S subunit structure in the same year 2000. One is at 3.3 Å resolution (31) and the other is at 3.05 Å resolution (32). This 3.05 Å resolution structure is the complete atomic model of 30S subunit. These structures helped in studying the interactions of antibiotics (33) and other functional ligands and factors with the subunits. In 2001, 70S ribosome at 5.5 Å resolution have been reported that was based on the model of RNA and protein backbone of 50S and 30S subunits structures described above (34).

This 70S ribosome structure was a complex with mRNA and tRNA molecules in P and E sites. There is another 70S ribosome structure reported at almost the same time with 6.5 Å resolution having all the A site, P site and E site t RNA molecules. This structure lost some of the diffraction but shows relative orientation of these tRNA molecules in the ribosome. The 70S structure with and without mRNA molecule has also been determined (34).

Translation: Protein synthesis occurs in amino to carboxyl terminal direction and mRNA is read from 5’ to 3’ direction and amino acids are added sequentially to the carboxy terminal end of the growing peptide chain (25, 26). These amino acids are brought in by aminoacyl tRNA molecules, which are modified with amino acids at their 3’OH end. This modification is

catalyzed by enzyme aminoacyl-tRNA synthetases. This step is very important since it is a proofreading step (25, 26).

Protein synthesis includes three steps; Initiation, elongation and termination. Initiation begins with the formation of ribosome around the first codon (AUG or GUG) in mRNA. This association of 30S subunit around the first codon is mediated by initiation factors, IF1, IF2 and IF3. First, purine rich sequence on mRNA (SD Sequence) is recognized by 16S rRNA of 30S subunit. This subunit contains all the initiation factors. IF3 is present on the interface (found in cryo EM studies but not in crystallography) in the E site (28). IF1 is present in the A site and increases the binding affinity of IF2 which then binds over IF1 in the A site. IF2 is the binding partner of fMet-tRNA^{fMet} (25, 26), IF3 helps in this selection of initiator tRNA by destabilizing any other tRNA in the P site (35). Once initiator tRNA binds in the P site of the ribosome, initiation factors start falling off and let 50S subunit bind and form entire 70S ribosome. This is now known as 70S initiation complex which is ready for elongation with fMet-tRNA^{fMet} in the P site and empty A and E site.

Elongation of peptide has three basic steps, peptide bond formation, elongation, and translocation (Fig 18). Since A site of the 70S initiation complex is empty, new aminoacyl tRNA is delivered to it as a ternary complex with elongation factor Tu (EF-Tu), a GTPase, and GTP. Codon and anticodon interaction occurs in the A site and correct pairing causes the conformational changes in the ribosome that triggers hydrolysis of GTP by EF-Tu (28). This leads to the release of EF-Tu from the A site. Proofreading occurs at this point to check if the base pairing is correct or not. This is most likely based on the conformational changes that are produced by correct pairing. Correct pairing induces the flipping of conserved purine bases in 16s RNA of 30S subunit and these flipped bases (A1492, A1493 and G530 (from syn to anti

conformation)) now interact with the minor groove of first two bases of the codon-anticodon bases (Fig 19) (36). This conformation leads to the conformational changes in EF-Tu and probably also in E site of the ribosome (36). As a result, EF-Tu hydrolyzes the GTP and releases from the ribosome due to its low affinity now. Also, E site deacylated tRNA leaves the ribosome as a result of these conformational changes. Immediately after the release of EF-Tu, 3' end of tRNA swings into the peptidyl center of the 50S subunit. This is followed by the peptide bond formation between the carboxyl group of P site tRNA amino acid and amino group of A site tRNA amino acid. It is clear from crystal structure of 50S subunit with Yarus inhibitor that this reaction is catalyzed by 23S

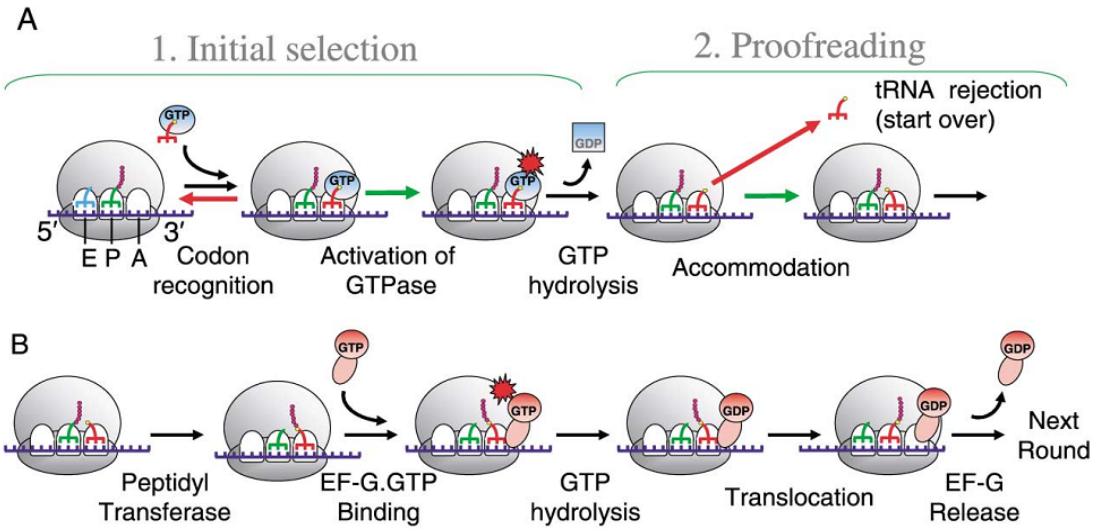

Fig 18. Overview of elongation cycle (V Ramakrishnan, Cell, Feb 2002).

RNA of peptidyl center of 50S subunit (29). This reaction is thermodynamically favorable and the catalysis occurs due to the suitable environment that is provided by three means (i) by precise orientation of A site and P site tRNA's CCA ends close to highly conserved A and P loops of 23S RNA, (ii) by transition state stablilization, and (iii) by direct involvement of two purines,

A2451 and G2447 in acid base catalysis that is required for the reaction (37). The crystal structure showed that A2451 is just 3 Å away from the A site tRNA amino acid and presumably hydrogen bonded with the A site tRNA (38). This residue needs to be protonated in order to make this hydrogen bond, leading to the proposal that it could accept proton from amino group of A site tRNA and donates it to 2'OH group of P Site tRNA. The position of A2451 is found consistent in several substrate bound crystal structure of 50S subunit and mutation of it results in a dominant-lethal phenotype (39). Following peptidyl transferase activity, P site has deacylated tRNA and A site has tRNA with one additional amino acid. In translocation, this P site deacylated tRNA moves to the E site and A site tRNA with new peptide moves into the P site preparing ribosomes for a new round of elongation. This movement (translocation) is a two step process, where 50S subunit moves first followed by 30S subunit movement in the same direction (40). This makes tRNA's in A and P site to remain in hybrid states (A site tRNA's CCA terminal in P site of 50S and A site of 30S, A/P hybrid state, and P site tRNA's CCA in E site of 50S and P site of 30S, P/E hybrid state) for a short time until 30S subunit moves (Fig 20). These states have been proved by footprinting experiments (41).

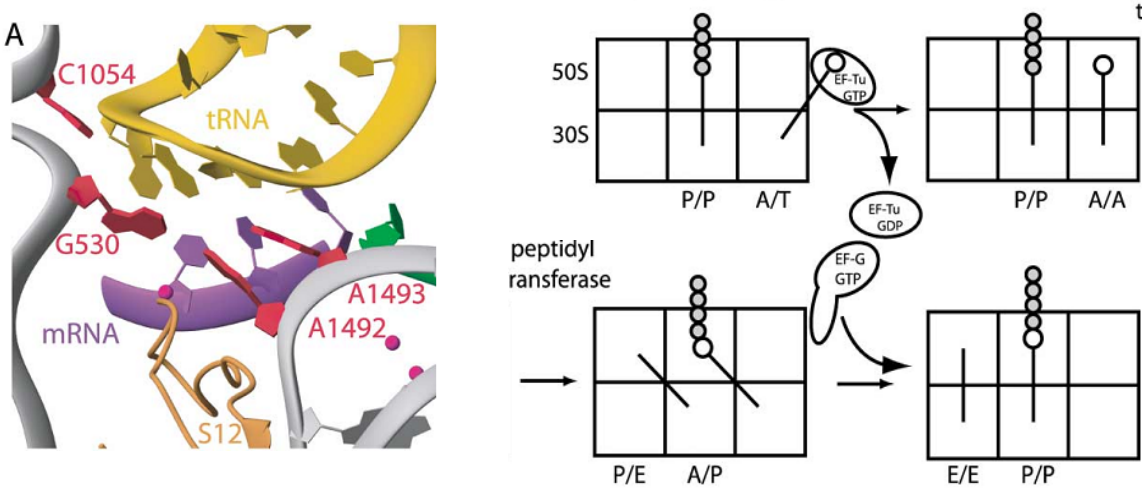

Fig 19. Codon-anticodon (Blue-Gold) base pairing. Critical bases of 16S RNA (Magenta) that stabilizes tRNA-mRNA complex (V Ramakrishnan, Cell, Feb 2002)

Fig 20. Translocation model as proposed by Moazed and Noller, 1989 (V Ramakrishnan, Cell, Feb 2002).

These experiments have also shown that EF-Tu bound amino acyl tRNA in the A site is also in a hybrid state T/A (T is the testing site), it is only after base pairing and EF-Tu release that it comes in A/A state. This translocation results in the ribosome having deacylated tRNA in the E site, peptidyl tRNA in the P site and empty A site for a new round of elongation.

The last and final step of translation is termination. Termination occurs when ribosomal A site reaches to one of the three termination codons on mRNA; UAA, UAG, or UGA. In bacteria, class I release factor recognizes these codons; for ex, RF1 recognizes UAA and UAG and RF2 recognizes UAA and UGA codons. Once release factors occupy the A site of the ribosome, class II release factor RF3, a GTPase, forms the complex with RF1/RF2. RF1/RF2 then causes hydrolysis and peptide chain release from the P site tRNA (28). It is not known if this hydrolysis is catalyzed by release factors or by conformation changes in the ribosome itself. This hydrolysis and peptide chain release then induces GTP binding to the RF3 and subsequently increases affinity of RF3 to the ribosome and releases RF1/RF2. GTP hydrolysis then leads to the release of RF3 due to decrease in its affinity to the ribosome. Entire mechanism of how exactly release factors recognize the codon in the A site and what conformational changes this recognition causes to induce hydrolysis and peptide chain release is not yet known completely.

CHAPTER II

MATERIALS AND METHODS

Small and Large Colloids: Small and large colloids were prepared according to ref 42 with slight modifications. Trisodium citrate (2 ml at 34 mM) was added dropwise to a stirred solution of $AgNO_3$ (100 ml at 1 mM) at 90 °C. The reaction mixture was heated to 90–95 °C, and stirring was continued for 15 min or until the reaction mixture turned pale yellow. For large colloids, the trisodium citrate was added in 4 aliquots of 0.5 ml each every 15 min. The resulting mixture was then incubated in an ice bath for 15-20 min. The small and large colloids were then purified by centrifugation three times at 8000 and 3500 rpm respectively for 8 min each time; the precipitate was then suspended in 1 ml of 1 mM trisodium citrate.

Buffers: All single molecule experiments were carried out in TAM_{15} buffer (20 mM Tris-HCl (pH 7.5), 15 mM $Mg(OAc)_2$, 30 mM NH_4Cl, 70 mM KCl, 0.75 mM EDTA, 1 mM DTT, and 0.2% (w/v) Tween 20). A deoxygenation enzyme system of 3 mg/mL glucose, 100 µg/mL glucose oxidase (Sigma-Aldrich), 40 µg/ml catalase (Roche), and 1.5 mM 6-hydroxy-2,5,7,8-tetramethyl-chromane-2-carboxylic acid (Trolox, Sigma-Aldrich), initially dissolved at 150 mM in DMSO, was added during single-molecule measurements to decrease photobleaching and photoblinking.

Proteins: Double variant of L11, C38S/S87C was prepared as described in ref 43. C38S/S87C-L11 was purified on a Ni-NTA column and then purified again essentially to homogeneity on a MonoS™ (5/50 GL) FPLC column (in buffer B with a linear gradient of 100 – 800 mM NH_4Cl).

Labeling of C38S/S87C-L11 with Cy3 was then performed by adding 50 µL of 10 mM Cy3-maleimide DMF, to C38S/S87C-L11 (in buffer C, 50 mM Tris-HCl pH 7.5, 400 mM NH_4Cl) with continuous stirring. The mixture was incubated at 37°C for 1 hour, and quenched with 3 µL of 14.3 M BME. Excess dye was removed via gel filtration on a Sephadex G-25 column, and the labeled protein was stored in buffer D (20 mM HEPES (pH 7.6), 400 mM NH_4Cl, 20 mM $MgCl_2$, 1 mM EDTA, 1mM DTT). Typical Cy3/L11 ratios were 0.9 ± 0.3. Cy3 was measured by absorbance at 550 nm and L11 was determined using the corrected Bradford assay (44).

Ribosomes: $70S^{Cy3}$ ribosomes were prepared by incubating a 2-fold molar excess of C38S/S87C-$L11^{Cy3}$ with 2 µM AM77 ribosomes lacking L11, in buffer E [50 mM Tris-HCl (pH 7.5), 70 mM NH_4Cl, 30 mM KCl, 20 mM $MgCl_2$, 1 mM DTT] for 15 minutes at 37°C (43, 44). Excess dye was then removed by centrifugation (400,000g, Sorvall Discovery M120SE) through a sucrose cushion (1.1 M sucrose in buffer E) at 4 °C for 40 minutes, yielding a ribosome pellet with Cy3/ribosome ratio of 0.8:1.0.

tRNAs: fMet-$tRNA^{fMet}$(Cy5), Arg-$tRNA^{Arg}$(Cy3), Arg-$tRNA^{Arg}$(Cy5), and Phe-$tRNA^{Phe}$(Cy5) were prepared using the reduction, charging, and labeling protocol described in ref 45. Separations of fMet-$tRNA^{fMet}$ from $tRNA^{fMet}$ and Phe-$tRNA^{Phe}$ from $tRNA^{Phe}$ were achieved by reversed-phase HPLC using a LiChrospher WP-300 RP-18 (5µm) column (250-4mm) (Merck KGaA-Darmstadt). The tRNA mixture was dissolved in buffer A5 (20 mM ammonium acetate [pH 5.0], 10 mM magnesium acetate, and 400 mM NaCl) and applied to the column equilibrated with buffer A5. Poly A was eluted with a linear gradient of buffer A5 to 20% buffer B5 (Buffer A plus 30% [v/v] ethanol). tRNAs were eluted by a linear gradient from 20% buffer B5 to 40% buffer B5. The same column was used to separate Phe-$tRNA^{Phe}$(Cy5) from unlabeled Phe-$tRNA^{Phe}$ and Arg-$tRNA^{Arg}$(Cy3) or Arg-$tRNA^{Arg}$(Cy5) from unlabeled Arg-$tRNA^{Arg}$. Here the

tRNA mixture is dissolved in buffer A6.5 (same as A5 but adjusted to pH 6.5), applied to the column equilibrated with buffer A6.5 and eluted by a linear gradient from buffer A6.5 to 100% buffer B6.5 (same as B5 but adjusted to pH 6.5). fMet-tRNA^{fMet}(Cy5) was purified in a similar fashion, but using buffers A5 and B5 to optimize the recovered charging stoichiometry. Partial resolution of Arg-tRNA^{Arg} from tRNA^{Arg} was achieved by FPLC (MonoQ) (45), which also removed polyA.

mRNA: The following mRNAs, purchased from Dharmacon, were used. mRNA: 5'-biotin labeled- GGG AAU UCA AAA AUU UAA AAG UUA AUA AGG AUA CAU ACU *AUG CGU UUC UUC CGU UUC UAU CGU UUC*. The underlined sequence is a strong Shine-Dalgarno region and italized sequence codes for MRFFRFYRF.

Complex Formation: 70S initiation complex was formed by incubating 1 µM 70S ribosome, 4 µM 5'-biotinylated mRNA, 1.5 µM each of IF1, IF2, IF3 and fMet-tRNA^{fMet}, and 1mM GTP in TAM_{15} buffer for 25 min at 37 °C. Ternary complex was formed by incubating 4 µM EF-Tu, 2 µM dye-labeled and charged tRNA, 3 mM GTP, 1.3 mM phosphoenolpyruvate, and 5 mg/L pyruvate kinase in TAM_{15} buffer for 15 min at 37 °C.

Immobilization Method: Pre-cleaned glass coverslips (Fisher Scientific) were aminosilanized by 3-aminopropyltriethoxysilane (United Chemical Technologies, Inc.). Colloids were then reacted with the aminosilane surface for 3 hr. Ag group of the colloidal particles react with free NH_2 group of aminosilane that is covalently bound to the glass surface. Colloidal coverslips were then incubated with polyethylene glycol (PEG, Laysan Bio, mixture of 5000 MW PEG-succinimidyl valerate and biotin-PEG-succinimidyl valerate at a molar ratio of 100:1 unbiotinylated:biotinylated PEG) for 3 hr. The following solutions were applied for 3 min

followed by a wash with TAM_{15} buffer. Streptavidin solution (0.5 mg/mL), biotinylated initiation complex solution (1-10 nM), and lastly EF-Tu/tRNA ternary complex (10 nM) to form an immobilized initiation (pre-translocation) complex. The translocation reaction was started by injecting 2 µM EF-G and 3 mM GTP. All single molecule studies were carried out at 21 °C.

Fluorescence intensity, FRET, and function of ribosomes were compared on slides containing colloidal silver particles as above with corresponding measurements on identically prepared slides except the colloids were not applied. In the text, the slides without colloids are termed "plain glass" but all of the layers except the colloids were the same.

TIRF measurements on immobilized ribosomes: A custom-built objective-type total internal reflection fluorescence (TIRF) microscope was based on a commercial inverted microscope (Eclipse Ti, Nikon) with a 1.49 N.A. 100x oil immersion objective (Apo TIRF; Nikon, Tokyo, Japan). Direct excitation (for fluorescence enhancement experiments) or Alternating-Laser EXcitation (ALEX) (46) (for FRET in activity assays) was used with a 532 nm laser (CrystaLaser, Inc.) and a 640 nm laser (Coherent, Inc.) to obtain Cy3 and Cy5 fluorescence intensities, and the FRET signal between Cy3 and Cy5. Fluorescence emission from Cy3 and Cy5 were separated by a Quad View splitter (Photometrics, Tucson, AZ) and recorded with an electron multiplying charge-coupled device (EM-CCD) camera (Cascade II, Photometrics) at 100 ms integration time.

For recording, several areas of 50 x 50 µm each were scanned from different slide chambers. Single molecules were then selected on the basis of single step photobleaching to avoid colloidal luminescence and intensities were calculated by fitting the intensity distribution to 2D Gaussian profiles within a 9 x 9 pixel area

$$f(x,y) = Ae^{-\left(\frac{(x-x_0)^2}{2\sigma_x^2}+\frac{(y-y_0)}{2\sigma_y^2}\right)}$$ Equation 1

where, A is the amplitude, x_0, y_0 is the center and σ_x, σ_y are the x and y standard deviations of the intensity distribution. The total number of camera digitizer units in the image (the intensity) was calculated as $I = 2\pi A\ \sigma_x,\ \sigma_y$ For fluorescence enhancement studies, intensities were then converted into number of photons using camera gain that was measured for CCD camera by procedure described in the next section. For FRET measurements, intensity traces were directly used and the FRET efficiency was calculated using equation 2

$$E = \left(1 + \frac{I_D}{I_A - \chi I_D}\gamma\right)^{-1}$$ Equation 2

where I_D is fluorescence intensity of donor, I_A is fluorescence intensity of acceptor, χ is cross-talk of donor into acceptor channel, and γ accounts for the differences in quantum yield and detection efficiency between the donor and the acceptor. γ is calculated as the ratio of change in the acceptor intensity, ΔI_A to change in the donor intensity, ΔI_D upon acceptor photobleaching or change of FRET efficiency ($\gamma = \Delta I_A / \Delta I_D$) (47, 48).

Camera gain measurement: The gain of the EM-CCD camera was measured in order to calculate the conversion factor relating the spot intensities to the number of collected photons. Measured pixel intensity A is related to the number of photons, N, by $A = Q\ N\ C\ /\ B$, where Q = quantum yield of the camera detector, C = gain (output current/input current) of the camera electron multiplier, and B = number of electrons (after the cascade amplifier) converted to each digital intensity unit (ADUs). B is often termed "Gain" in EM-CCD camera literature. The

variance (V) of a pixel intensity is given by $V = 2\ Q\ N\ C^2\ /\ B^2$, where the factor of 2 is an approximation of the excess noise introduced by the cascade amplifier. Values of variance and intensities were obtained by measuring pixel intensities over time with a stable light source, or from successive difference images. Plots of V vs. A were linear with slope ($V\ /\ A = 2\ C\ /\ B$) corresponding to $C\ /\ B = 70$ at the experimental cascade amplifier setting. Taking Q as 0.9 from the camera specifications, the ratio of pixel output signal to number of collected photons is thus 63.

Hammy: The Hidden Markov Model based software HaMMy (49) was used to analyze the FRET traces. The software was set to look for two FRET states. The traces with only one FRET state were considered to be stable traces, whereas the traces with two FRET states were considered to be fluctuating traces. Dwell times of high and low FRET of fluctuating traces were calculated by HaMMy and fitted to a bi-exponential curve:

$$P = A_1 \exp(-k_1 t) + A_2 \exp(-k_2 t)\,. \qquad \text{Equation 3}$$

AFM: An atomic force microscope (MFP 3D-BIO Model, Asylum Research, Inc.) was used to characterize the size of colloidal silver particles. Silver particles were prepared and deposited as described above and dry sample imaging was performed in tapping mode. An AC 240TS cantilever with resonant frequency ~60 kHz was used. The AFM system was integrated with an inverted objective-type TIRF microscope similar to the instrument described earlier, based on a Nikon Eclipse Ti platform and a 1.49 N.A 100x (Apo TIRF; Nikon, Inc.) oil immersion

objective. For data analysis of the AFM images, we used Igor-based MFP 3D and ARgyle Light softwares.

CHAPTER III

SPECIFIC AIMS

Fluorescence technology is applicable to a wide variety of biological research and medical/clinical diagnostic questions (1, 2). In the last decade, single molecule fluorescence (SMF) detection has been developed to selectively address individual molecules in order to detect processes that are hidden in ensemble measurements and to avoid averaging effects (9-14). SMF has been used to study many molecules involved in cellular processes including the motions of molecular motors (50-54), transcription (55, 56), and translation (44, 57, 58). In single molecule fluorescence studies of localization or orientation, the target macromolecule is labeled with an organic fluorophore, such as rhodamine, cyanine dye, or a semiconductor quantum dot (QD), or ligated to a variant of green fluorescent protein (59-61). For distance measurements and dynamics, these probes are often used in pairs (e.g. Cy3 and Cy5) that exhibit distance-dependent Forster Resonance Energy Transfer (FRET).

However, low emission intensity, fluctuations and photobleaching of organic fluorophores and fluorescent proteins often limit the signal-to-noise characteristics of SMF measurements (16, 17). The local environment of the probe on the macromolecule, the imaging buffer and its oxygen content, and the illumination intensity all strongly influence photostability. Stronger illumination increases fluorescence intensity usually with a proportional worsening of the photobleaching rate.

Compared to the nanosecond timescale of photophysical reactions, microsecond and millisecond enzymatic processes are slow. For example; the peptide elongation cycle during protein synthesis occurs at the rate of 3-6 amino acids per ribosome per second *in vitro* (62) and 20 per second *in vivo* (63). Depending on the required excitation and fluorescence emission intensity, organic fluorophores may photobleach after only a few elongation cycles, long before an entire protein is synthesized. The tradeoff between intensity and photobleaching thus undermines the power of SMF in determining reaction mechanisms, especially for highly processive enzyme systems.

Brighter and more photostable fluorophores or processes that can enhance the fluorophore's emission intensity are advantageous to increase the rate of photon collection and/or reduce the excitation laser intensity. Quantum dots are very bright and resistant to photobleaching; however they are physically larger than organic fluorophores (5-10 nm diameter) and they blink extensively (18).

Another approach is to use surface plasmons of noble metals to engineer the spectral properties of fluorophores to enhance their fluorescence (19). Coupling between the fluorescence resonance of the fluorophore and the plasmon resonance of nearby metal particles forms an oscillating dipole that increases the radiative rate of fluorescence (20-22). This phenomenon is termed metal-enhanced fluorescence (MEF). While they are in the electronically excited state, fluorescent probes are susceptible to photophysical reactions that cause them to blink and bleach (23, 24). Thus increasing the rate of fluorescence emission increases brightness, while also improving photostability and reducing blinking (23, 24).

Although MEF has huge potential in determining long molecular and cellular processes but till date it has only been shown to have enhancing fluorescence of either bare dyes or small protein

molecules at both ensemble and single molecule levels. But in order to elucidate most of the cellular processes, complex biological molecules are needed to be labeled and fluorescence enhancement of these molecules using MEF would be extremely useful. Unfortunately, there are rare studies where such complex biological molecules have been used, for example; supramolecular complexes. Moreover, even if these supramolecular complexes show enhanced fluorescence signals it would be hard to elucidate their dynamics or any functional process since not all the biological molecules are active near the metal surfaces (64). So, we designed this study to address these issues and our specific aims are following:

Specific Aim 1: To characterize silver colloidal particles and determine if they are suitable for single molecule studies of supramolecular complexes, ribosomes.

Specific Aim 2: To check the fluorescence enhancement of Cy3 and Cy5 labeled initiation complexes (ICs).

Specific Aim 3: To check if these initiation complexes are biologically active near metal particles while having enhanced fluorescence

CHAPTER IV

SPECIFIC AIM 1

<u>Specific Aim 1</u>: To characterize silver colloidal particles and determine if they are suitable for single molecule studies of supramolecular complexes, ribosomes.

Rationale:

As discussed, silver colloidal particles have mainly been used for ensemble studies but rarely for single molecule studies. Hence, it is not very well known if these metal particles are suitable for single molecule studies. Moreover, this suitability needs to be checked for a particular set of optics in the given instrument before any study since different excitation and emission collection methods could affect the results. Most importantly, we wanted to know if backscattering, reflection and any emission from these colloidal particles interfere in the efficiency of collecting fluorescence signals from single molecules. Also, if we could resolve our fluorescence signal (from single molecules) from any unwanted signals from the colloidal particles. Therefore, we wanted to characterize these colloidal particles.

Results:

Colloidal silver particles, prepared by reducing silver nitrate with sodium citrate, were attached to glass microscope slides as described in Methods. Two sizes of particles were made by varying the rate of reduction. The size of the silver particles was measured using AFM giving average diameters of 50 ± 16 and 85 ± 18 nm (mean ± s.d., n = 463 and 789) from the heights of

the small and large particles respectively (Fig. 1). Some of the particles aggregated into larger spherical or rod shaped structures which are evident in the AFM images. We noticed that surfaces coated with colloidal particles and illuminated by visible laser light emitted luminescence, shifted to longer wavelengths. This luminescence has been described before (65-67) and ascribed to resonant extinction (resonant scattering and absorption) between two colloidal particles spaced more closely than their diameter (65-67). As such emission would interfere with detection of single fluorophores on a biological sample, we further characterized it.

Particles at low density were illuminated by 532 nm laser light in TIRF mode and images were collected in orange (550 – 620 nm), and deep red (660 – 720 nm) emission channels on an EMCCD video camera (Fig. 2A and 2B). Backscattered 532 nm light (Fig. 2C, no emission filter, camera gain reduced to minimum) was imaged to detect the position of the silver particles (68). Luminescence was detected in both of the long wavelength detector channels from some of the particles (~15 % and ~4%) detected by scattering and AFM imaging respectively (Fig. 2).

We used a TIRF microscope integrated with an AFM system (Methods) to determine whether the size of the particles affected the luminescence. Regions of the slide were imaged by TIRF microscopy using 540 nm laser light and scanned by AFM (Fig. 2d and 2e respectively). The two images were scaled, registered with each other and merged using ImageJ and Matlab scripts. All of the luminescent spots could clearly be identified with objects in the AFM images (Fig. 2f), showing that the luminescent spots in both the orange and red emission channels originated at silver colloidal particles. Not all the silver particles detected by AFM produced appreciable luminescence. Most of the luminescent spots were located at an area of the AFM image containing several silver particles or an aggregate (Fig. 2d and 2e), as expected if larger silver colloids were more luminescent than smaller ones. From size distributions of particles that

produced luminescence (Fig. 3a) and the total population (Fig. 3b), we determined that 98% of the particles producing luminescence are 250 μm^3 or larger, although not all particles above this volume produced detectable luminescence. The proportion of particles that produce luminescence and the luminescent intensity depends strongly on the particle size (Fig. 3c). These results are compatible with the resonant extinction emission mechanism described earlier (65-67).

Next, we determined the relative luminescence from 50 nm and 85 nm diameter silver particles in the two camera fluorescence detector channels. Intensities were collected from 30 or more particles. The larger particles have ~3-fold more luminescence compared to the smaller ones when excited at either 532 nm or 640 nm with detection at 585 nm or 690 nm, respectively, and ~5-fold more luminescence when excited at 532 nm laser with detection at 690 nm (Table 1). Thus, as expected from the resonant extinction mechanism, the emission of the larger particles is greater and extends to longer wavelengths.

The wavelength-shifted luminescence from silver particles either does not photobleach or else bleaches slowly and gradually, whereas single organic fluorophores used for biological labeling photobleach in a single step. As a result, stepwise photobleaching to a steady background enables fluorophores to be distinguished from colloidal luminescence at the site of a colloidal particle.

Figures

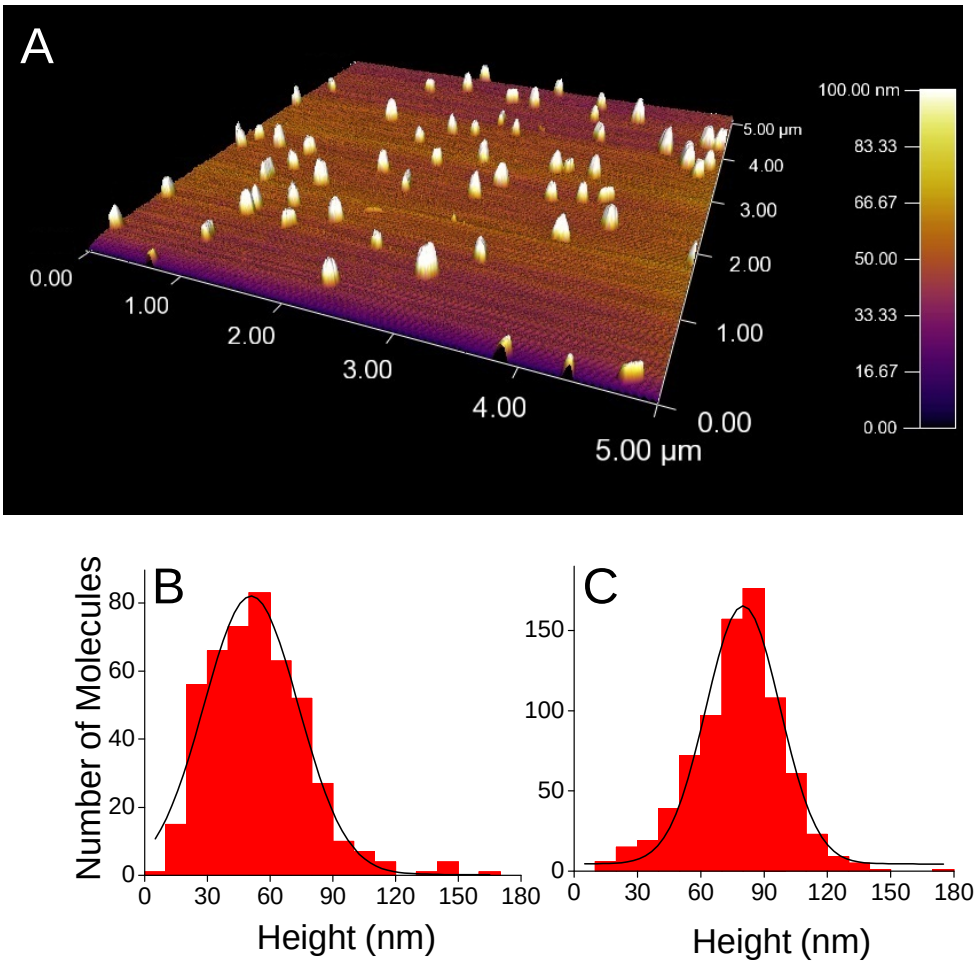

Fig 1 AFM 3-D renderings of colloidal silver particles (A) and the size distribution of small (B) and large (C) silver particles.

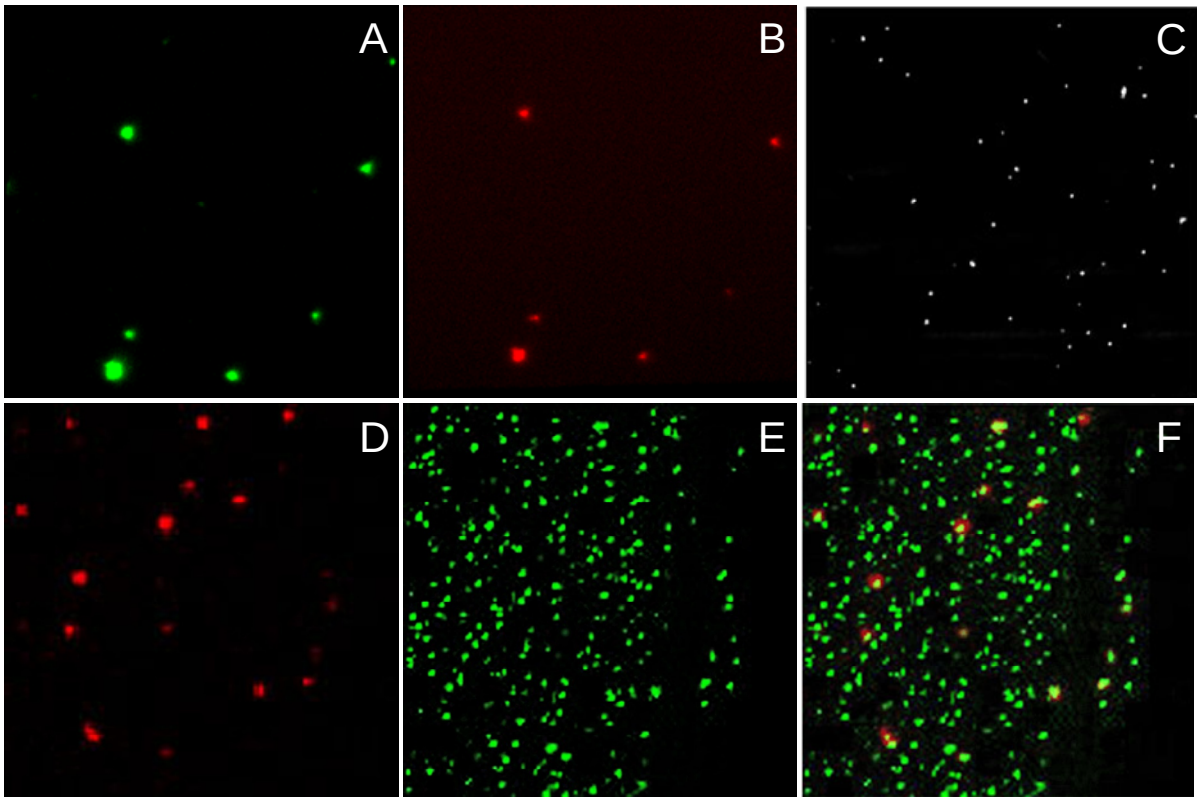

Fig 2 Imaging of small silver particles. Long wavelength shifted luminescence images in green (550-620 nm) channel (A), red (660-720 nm) channel (B), and scattering image (C) of small silver particles. Long wavelength shifted luminescence image in red channel (660-720 nm) (D), AFM image (E) and merged luminescence-AFM image (F) of silver particles.

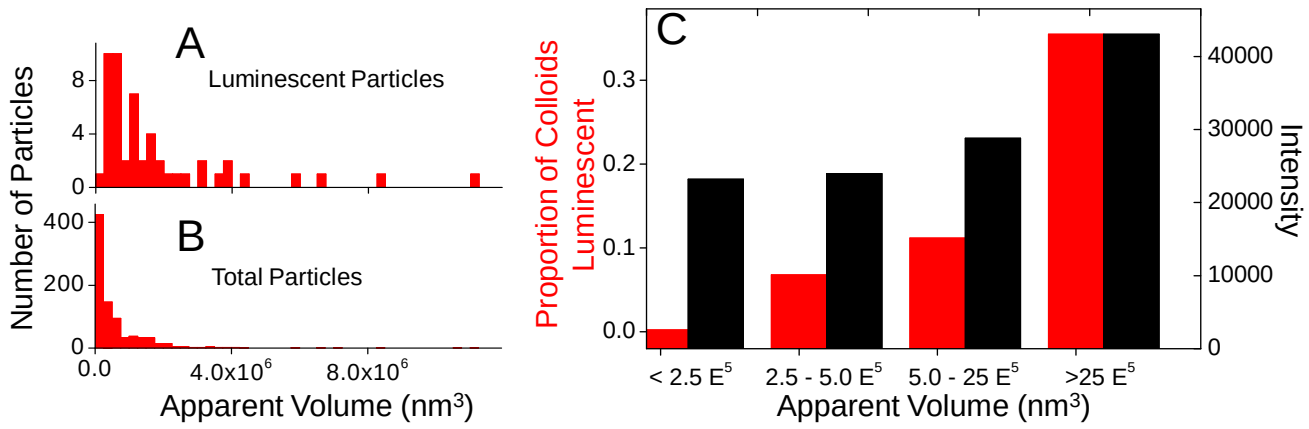

Fig 3 Apparent volume distributions of luminescent silver particles (A) and total silver particles (B) from same region. Dependence of proportion of silver particles having luminescence and their intensity on apparent volume of silver particles/aggregates (C).

Excitation/Emission Wavelengths	Small Colloids	Large Colloids
532 nm/585 nm	8437 ± 834	25152 ± 3306
640 nm/690 nm	6678 ± 783	18040 ± 3041
532 nm/690 nm	4023 ± 448	19610 ± 3183

Table 1. Average luminosity values of small and large colloidal particles when illuminated by 532 or 640 nm laser light and detected in orange (585±35 nm) or red (690±30 nm) emis sion channels. Intensity measurements are means ± SEM of 30 or more particles.

CHAPTER V

SPECIFIC AIM 2

Specific Aim 2: To check the fluorescence enhancement of Cy3 and Cy5 labeled initiation complexes (ICs).

Rationale:

Although Metal Enhanced Fluorescence (MEF) has huge potential in determining long molecular and cellular processes but till date it has only been shown to have enhancing fluorescence of either bare dyes or small protein molecules at both ensemble and single molecule levels. In order to elucidate most of the cellular processes, complex biological molecules are needed to be labeled and fluorescence enhancement of these molecules using MEF would be extremely useful. But metal particles might not be as effective in enhancing fluorescence on larger complex molecules as for smaller ones. Hence, here we wanted to test the aspects of metal enhanced fluorescence of organic fluorophores bound to components of supramolecular complexes like ribosomes, tRNAs, parts of the protein synthesis machinery.

Results:

Because the smaller, 50 nm silver particles produced less resonant emission, this material was used to characterize the enhancement of fluorescence from Cy3 and Cy5 probes. Ribosomes were attached to the microscope slides through a short biotinylated test mRNA linked to a layer of polyethylene glycol (PEG) covering sparsely distributed colloidal particles (Methods).

Ribosomal initiation complexes (ICs) were labeled specifically with Cy3 or Cy5 on the large subunit protein L11 (44), or pre-translocation complexes contained Cy5-labeled arginine tRNA bound to the A-site. The labeled ribosomes attached to the surface via a biotinylated mRNA, randomly with respect to the silver particles. The Cy3- or Cy5-labeled complexes were excited in TIRF mode by green (532 nm) or red (640 nm) lasers, respectively. Single molecules were selected on the basis of single step photobleaching to avoid interference from colloidal luminescence, as described above, and intensities were calculated by fitting 2D Gaussian profiles to the intensity distributions as described in Methods.

Comparison of fluorescence micrographs of Cy3-labeled initiation complexes bound to PEG-coated glass slides without and with silver particles (Fig. 1a and 1b, respectively) shows clear enhancement of fluorescence intensity by the colloidal particles. The median intensity on plain glass was 3,900 camera intensity units, with very few spots having intensities higher than 10,000 units (Fig. 1c). In contrast, a large proportion of the single molecule complexes had intensities of >10,000 units on slides containing silver particles (Fig. 1d). As determined from the quantum yield of the camera and its gain (measured as described in Methods), 10,000 intensity units correspond to ~160 photons striking a camera pixel during each 100 ms recording period. The higher intensity spots in the presence of the colloidal particles are not aggregates of more than one labeled ribosome, because the fluorescence bleaches to the background level in a single step (intensity traces, Fig. 1e and f). As expected, quite similar results were found for Cy5-labeled initiation complexes (Fig. 2). The higher fluorescence on the colloidal particles often displayed 0.1 – 5 Hz fluctuations above photon counting shot noise, as in Fig. 1f and 2f. Noise in the traces on plain glass was slightly higher than expected from photon counting statistics, presumably due to excess noise of the camera gain multiplier and fluorophore photochemical processes. For ICs

colocalized with 50 nm silver particles, the noise above the expected shot noise was higher, 2 – 3-fold above shot noise (Table 1). After photobleaching of both Cy3 and Cy5 high intensity spots, the background intensity was slightly higher (~500 intensity units) than on plain glass, presumably due to resonance emission of the nearby colloid particle.

To confirm that enhancement of the fluorescence was due to the proximity of the ribosomes to the silver particles, we captured images of backscattered light from the silver particles and fluorescence from labeled ribosomes in the same area, registered the images to each other using Matlab and ImageJ scripts, and sorted the spots according to colocalization, within one pixel, with a silver particle. For Cy3-labeled ICs, this analysis showed that 83% of the molecules that were colocalized with a silver particle had high (>10,000) intensity compared to 1% of the spots on plain glass (Fig. 3a and 3b, respectively). The corresponding values for Cy5-labeled ICs were 72% and 2% (Fig. 3c and 3d respectively). Median intensities for the fluorophores colocalized with colloids (Table 1) were enhanced, 6.7- and 4.7-fold for Cy3 and Cy5, respectively, relative to values on plain glass.

Assuming that binding of ribosome ICs to the PEG coated surface was random, irrespective of whether a colloidal particle was nearby, the density of colloidal particles and the propotion of fluorophores with enhanced fluorescence allow an estimate of the area around a particle that leads to enhancement. The density of colloidal particles on the surface, detected by AFM was 2.3±0.3 per μm^2. 52% of Cy5 labeled complexes on the silver-treated slides exhibited high intensity (>10,000 camera units). These values lead to an area with apparent radius of 270 nm surrounding each particle that gave fluorescent enhancement. This value is very approximate because the density of colloids was measured by AFM on separate slides from the fluorescence ones, because light scattering identified fewer particles, presumably the larger ones.

For the fluorescence enhancement to be of practical benefit in a dynamic biophysical experiment, the total number of photons collected from the fluorophore before it photobleaches must be enhanced. Recording times before photobleaching of the fluorescence enhanced Cy3- and Cy5-labeled ICs close to silver particles were compared to ones bound to plain glass. The product of the recording time (determined by the rate of photobleaching) and the intensity gives a relative measure of the total number of photons captured. Under the present recording conditions, the average recording times for Cy3 and Cy5 labeled initiation complexes were slightly increased by the presence of silver particles (31 s for Cy3 near particles *vs*. 30 s on plain glass and 43 s for Cy5 near particles *vs*. 33 s on glass (Table 1, Fig. 4). The total number of photons emitted by Cy3- and Cy5-labeled initiation complexes (the products of intensity and recording time) were 4.2- and 5.5-fold higher on average, respectively, near silver particles compared to plain glass (Table 1, Fig. 3).

Due to higher scattering, large silver colloidal particles have been reported to produce greater enhancement of fluorescence than small ones (1). Median intensity was increased more(6.7-fold, Fig. 6, Table 2) on 85 nm particles than on 50 nm ones (4.7-fold, Fig. 3, Table 1). It is worth noting, however, that the average recording time before photobleaching was shorter near the 85 nm particles than the 50 nm particles (30s (Fig. 6d) and 43s (Fig. 4d), respectively). The enhancement of total number of photons collected from Cy5 near colloidal particles, above those on plain glass, was very similar on large particles (4.8-fold, Table 2) to that on small ones (5.5-fold, Table 1).

Figures

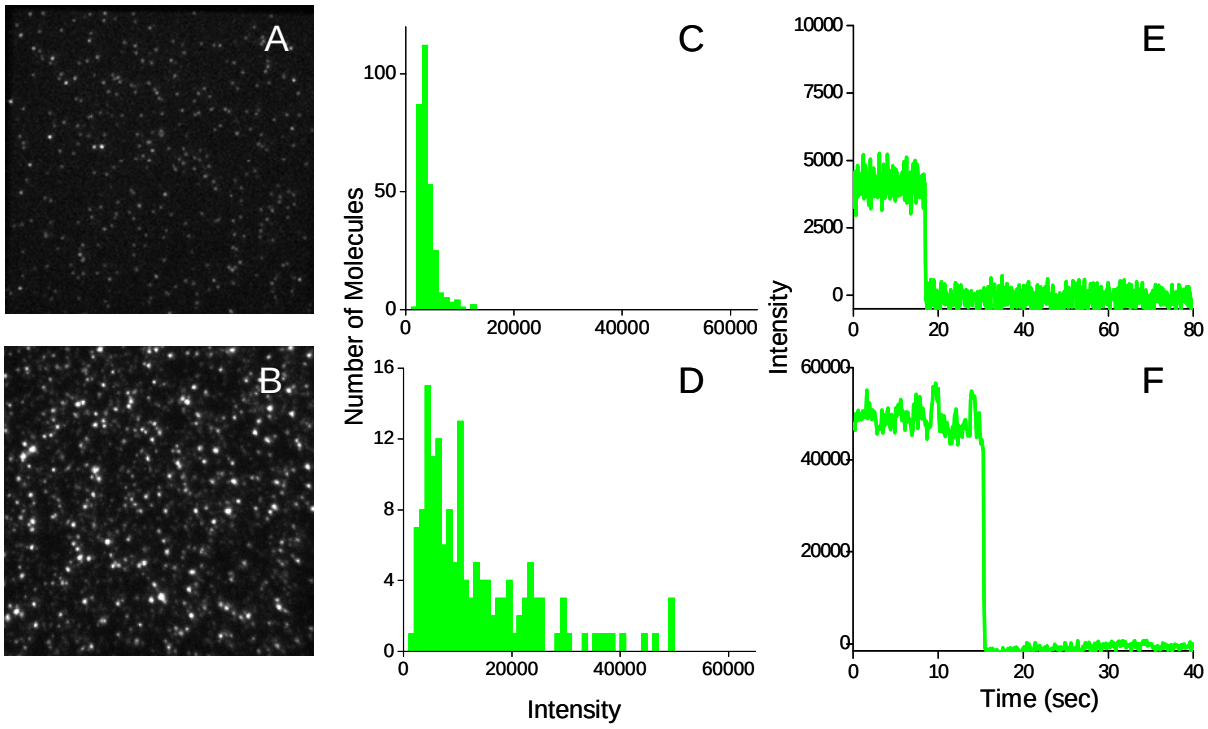

Fig 1 Comparison of Cy3 labeled initiation complexes (ICs) on plain glass and small silver particles coated glass surface. Fluorescence images of Cy3 labeled ICs on plain glass surface (A) and small silver particle coated glass surface (B). Intensity histograms of Cy3 labeled ICs on plain glass surface (C) and small silver particle coated glass surface (D). Single molecule traces of Cy3 labeled ICs on plain glass surface (E) and small silver particle coated glass surface (F).

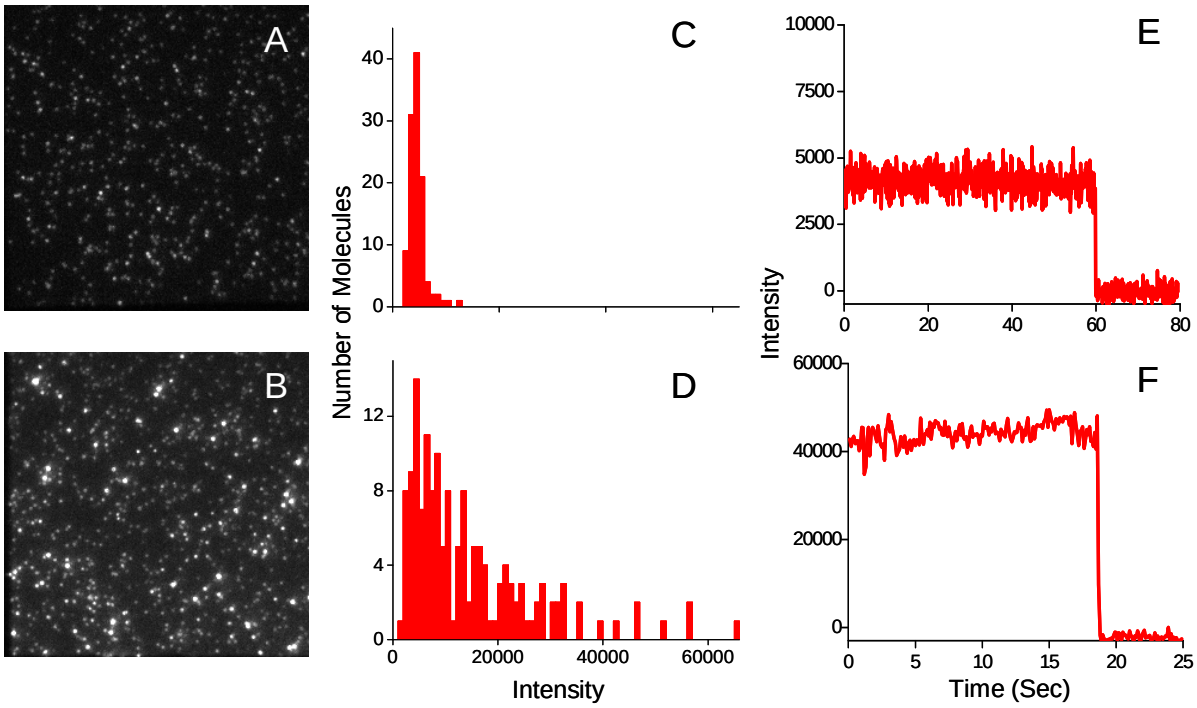

Fig 2 Comparison of Cy5 labeled ICs on plain glass and small silver particles coated glass surface. Fluorescence images of Cy5 labeled ICs on plain glass surface (A) and small silver particle coated glass surface (B). Intensity histograms of Cy5 labeled ICs on plain glass surface (C) and small silver particle coated glass surface (D). Single molecule traces of Cy5 labeled ICs on plain glass surface (E) and small silver particle coated glass surface (F).

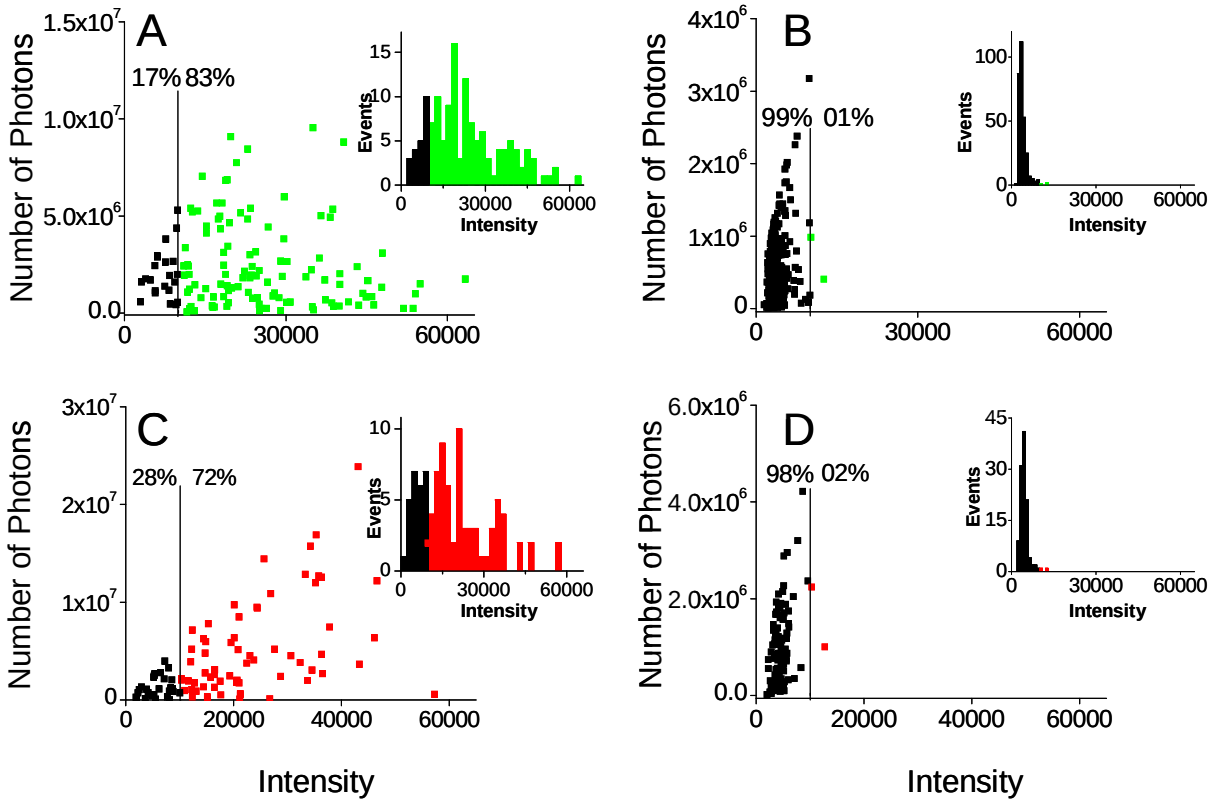

Fig 3 Photostability-intensity plots of Cy3 and Cy5 labeled ICs on plain glass and small silver particles coated glass. Number of photons emitted from each single spot before photobleaching vs. intensity of Cy3 labeled ICs, colocalized with silver particles (within 1 pixel) (A) and on plain glass (B), Cy5 labeled ICs, colocalized with silver particles (within 1 pixel) (C) and on plain glass (D). Intensity distributions for respective Cy3 and Cy5 labeled ICs are in the insets.

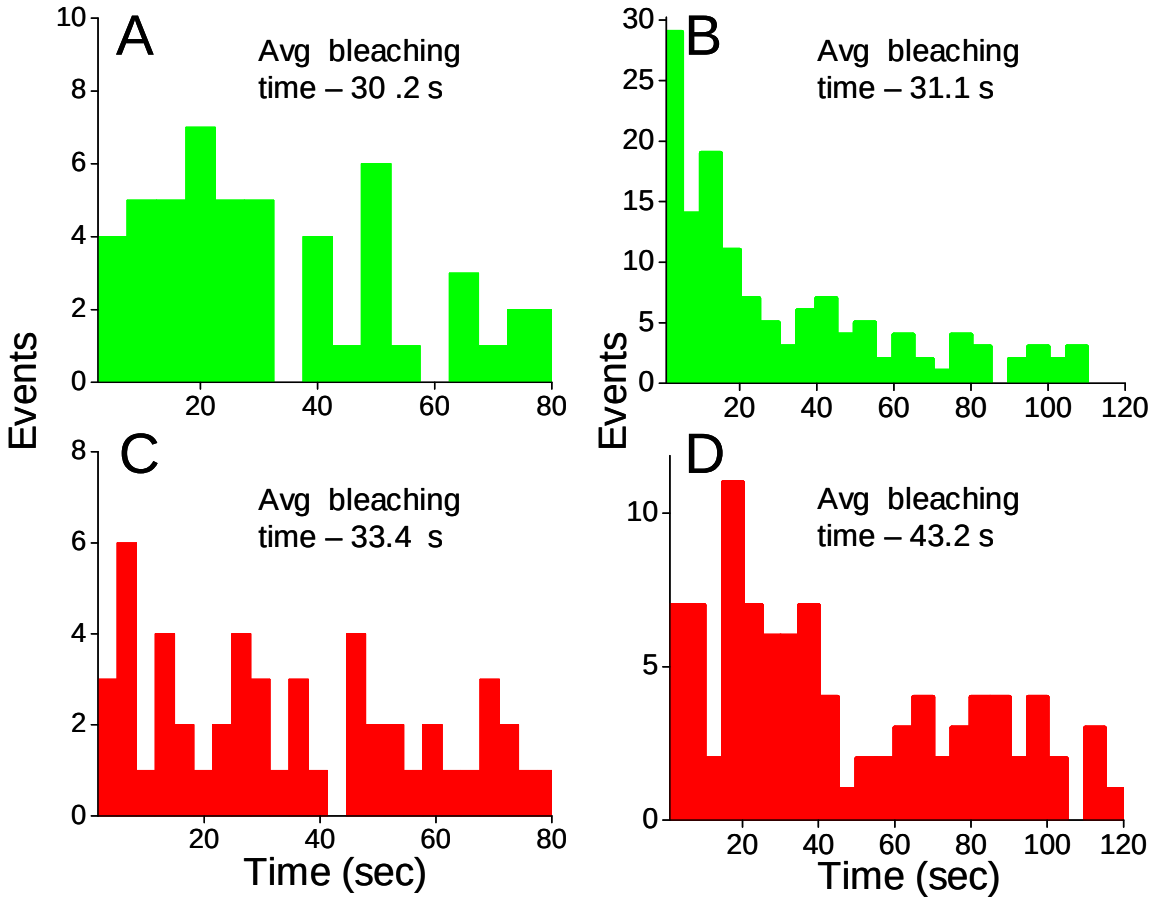

Fig 4 Photobleaching lifetime distributions of Cy3 and Cy5 labeled ICs on plain glass and small silver particle coated glass surface. Photobleaching lifetime distribution of (A) Cy3 labeled ICs on plain glass, (B) colocalized Cy3 labeled ICs with silver particles (within 1 pixel) on silver particle coated glass surface, (C) Cy5 labeled ICs on plain glass and (D) colocalized Cy5 labeled ICs with silver particles (within 1 pixel), on small silver particle coated glass surface.

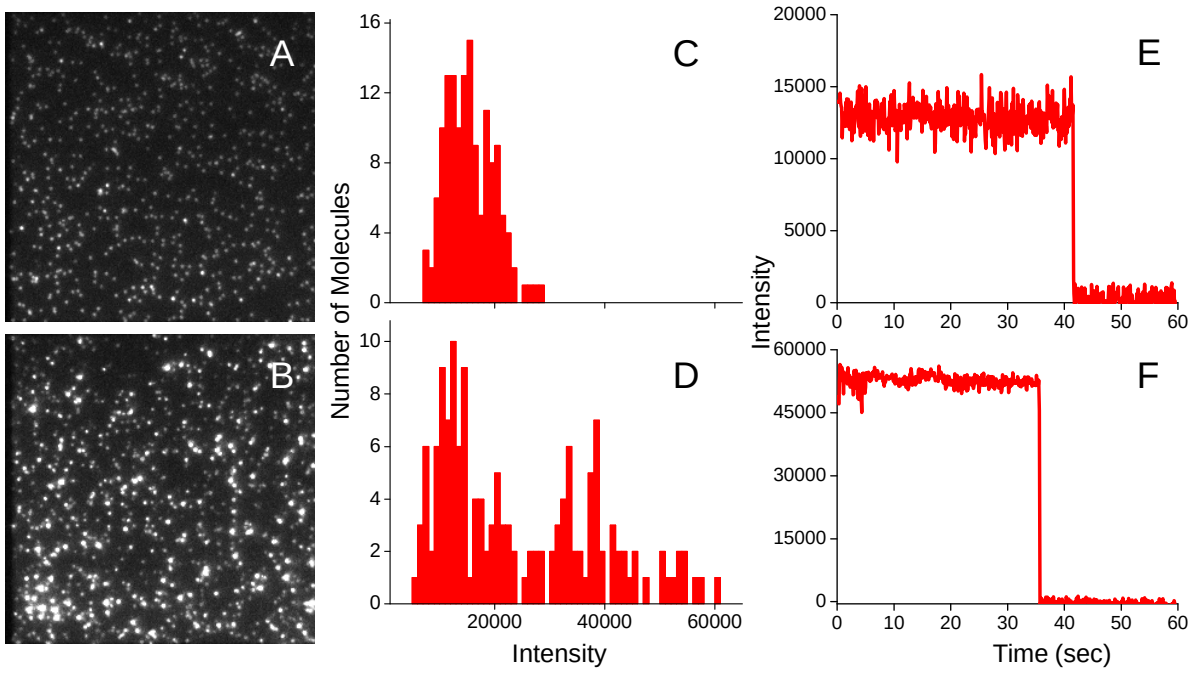

Fig 5 Comparison of Cy5 labeled ICs on plain glass and large silver particles coated glass surface. Fluorescence images of Cy5 labeled ICs on plain glass surface (A) and large silver particle coated glass surface (B). Intensity histograms of Cy5 labeled ICs on plain glass surface (C) and large silver particle coated glass surface (D) Single molecule traces of Cy5 labeled ICs on plain glass surface (E) and large silver particle coated glass surface (F).

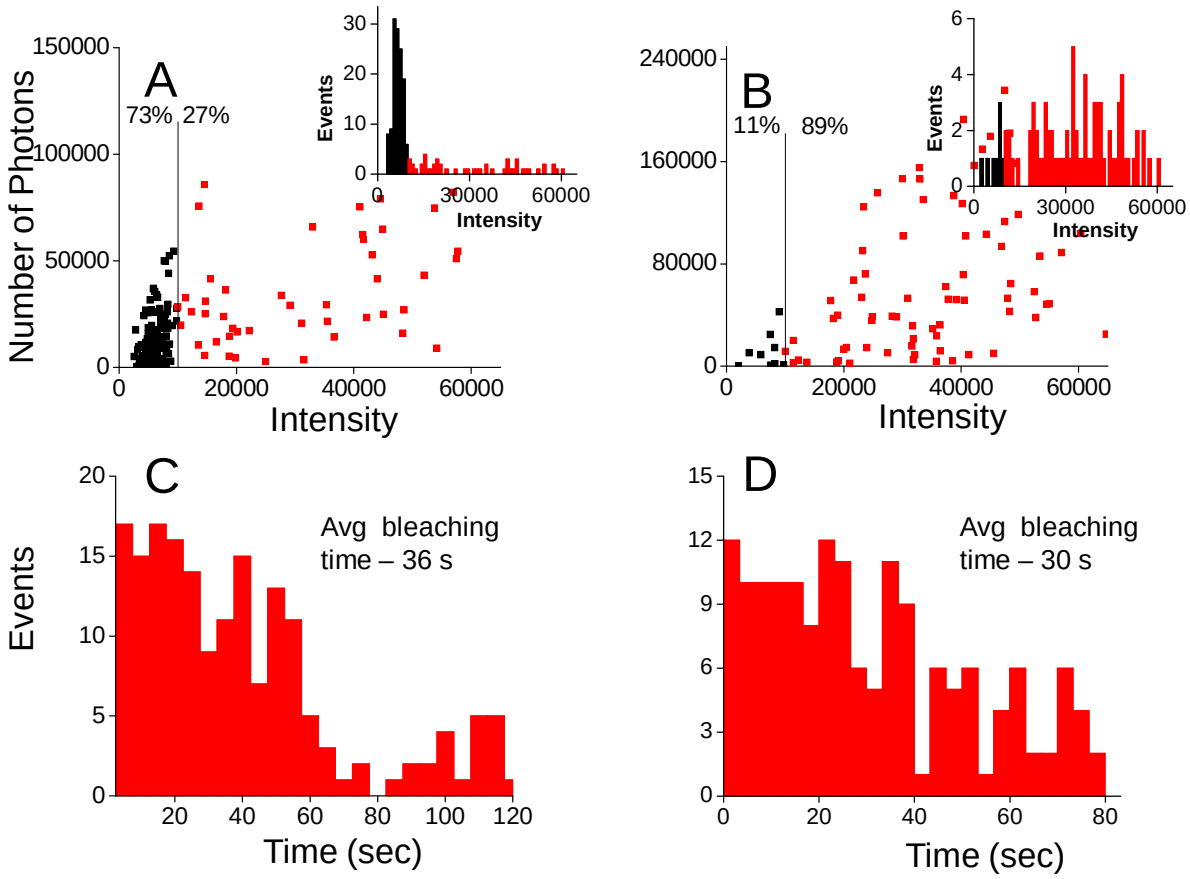

Fig 6 Photostability-intensity and Photobleaching lifetime distribution plots of Cy5 labeled ICs on large silver particles coated glass surface. Number of photons emitted from each single spot before photobleaching vs. intensity of non-colocalized Cy5 labeled ICs (A), colocalized Cy5 labeled ICs (B) with large silver particles (within 1 pixel). Intensity distributions for non-colocalized and colocalized Cy5 labeled ICs are in the insets of A and B respectively. Photobleaching lifetime distributions of non-colocalized (C) and colocalized (D) Cy5 labeled ICs on large silver particles.

	SURFACE	N	MEDIAN $x10^3$	MEAN $x10^3$	SD $x10^3$	BLEACHING TIME (s)	TOTAL PHOTONS $x10^5$	S/N	N/S	N_e/S
Cy3	GLASS	302	3.5	3.9	1.6	30	1.6	19	0.054	0.044
Cy3	COLLOIDS	115	23	26	12	31	6.9	29	0.035	0.017
Cy5	GLASS	113	4.4	4.6	1.6	33	2.7	20	0.049	0.039
Cy5	COLLOIDS	68	21	25	12	43	15	20	0.050	0.017

TABLE 1: Intensity distributions and noise of Cy and Cy5 labeled initiation complexes on glass and colocalized with small colloids. Mean and median intensity values are in camera A/D units, 10,000 ADUs = ~160 photons per pixel. Considering the widths of the intensity spots (σ_x and σ_y), total ADUs per molecule = 8.3-fold higher than the central intensity for Cy3 and 8.9-fold higher for Cy5. Bleaching time reports average recording time before bhotobleaching. Total photons collected were determined (using intensity, camera calibration and photobleaching time) from each recording and then averaged among traces. Signal to noise ratio (S/N) was calculated from Fourier transforms of the traces at 0.1 – 5 Hz. N/S is the reciprocal of S/N. N_e/S is the noise relative to signal intensity expected solely from Poisson counting statistics of the photoelectrons.

	SURFACE	N	MEDIAN $x10^3$	MEAN $x10^3$	SD $x10^3$	BLEACHING TIME	TOTAL PHOTONS $x10^5$	S/N	N/S	N_e/S
Cy5	GLASS	71	6.1	6.2	1.4	40	3.5	23.5	0.043	0.034
Cy5	COLLOIDS	128	41	40.5	12	29.5	17	13.4	0.075	0.013

TABLE 2: Intensity distributions and noise of Cy5 labeled initiation complexes on glass and colocalized with large colloids. Units and columns as in Table S2. Signal to noise ratios for plain glass are estimated.

CHAPTER VI

SPECIFIC AIM 3

Specific Aim 3: To check if these initiation complexes are biologically active near metal particles while having enhanced fluorescence

Rationale:

Single molecule studies using metal enhanced fluorescence have the advantage that they can be used in determining longer cellular and molecular processes that are otherwise difficult to be determined due to shorter lifetime of the fluorophores which hampers the studies. But such studies could only be done if the biological molecules remain unaffected close to the metal particles because not all the biological molecules are active in proximity of metal particles. Hence, even if the fluorescence of single fluorophore molecule, conjugated to the biological molecule, gets enhanced it will not be beneficial if the biological molecule itself is inactive. Therefore, in this specific aim, we wanted to check if the initiation complexes labeled with Cy3 and Cy5 dyes are active close to these metal particles while having enhanced fluorescence.

Results:

We checked whether initiation complexes (ICs) bound near to silver particles are active in binding Arg-tRNA^{Arg} at their A-site, forming the pre-translocation complex, and then if they translocate the resulting fMet-Arg-tRNA^{Arg} (dipeptide) in the A and P sites to the P and E sites.

First, we used unlabeled initiation complexes with fMet-Arg-Cy3-tRNA^{Arg} in the P-site and tested binding of Phe-Cy5-tRNA^{Phe} to the A site to form the pre-translocation complex. The coding mRNA sequence was *AUG CGU UUC UUC CGU UUC UAU CGU UUC* corresponding to MRFFRFYRF (single letter amino acid code), so that Phe-tRNA^{Phe} was the next codon-dependent binding partner. Of ~900 colocalized Cy3 and Cy5 molecules on the surface (collected from at least 6 different regions from two different experiments, Methods), 65% gave high Cy5 intensity (>10,000 counts for Cy5 upon direct excitation, assumed to be close to the silver particles) and 35% gave lower Cy5 intensity (≤10,000 counts, assumed to be away from silver particles). Of the high intensity colocalized spots, 21% showed FRET efficiency >0.35 between the two adjacent tRNAs, compared to 30% for lower intensity ones, suggesting that slightly fewer of the ribosomes are active in this assay near the silver particles than on PEG-coated plain glass.

We used the high and low intensity traces separately to calculate FRET efficiency values in the pre-translation complex and to compare with the FRET efficiencies measured from plain glass. The tRNAs adopt two conformations, assigned to so-called classic (A/A, P/P) and hybrid (A/P, P/E) states, leading to two peaks in distributions of FRET efficiency (69, 70). High intensity traces (near silver particles) gave components of FRET at 0.66 and 0.43 (Fig. 1), very similar to those of lower intensity traces, 0.65 and 0.36 away from the colloids (Fig. 2) and 0.62 and 0.36 on plain glass (Fig. 3). In many of the ribosomes, the Cy5-tRNA^{Arg} and Cy3-tRNA^{Phe} fluctuate between these two states. Time courses of anti-correlated Cy3 donor and Cy5 acceptor fluorescence intensities (Figs. 1, 2 and 3), show similar characteristics except for the higher total intensity near silver particles than for ICs away from silver particles. Dwell times at high and low FRET were 1.66 ± 0.1 s and 1.04 ± 0.06 s, respectively, for high intensity traces (Fig. 1d,e),

1.67 ± 0.04 s and 0.81 ± 0.03 s, respectively, for low intensity traces (Fig. 2d,e) and 1.34 ± 0.04 and 1.13 ± 0.03 s on plain glass (Fig. 3d,e) (mean ± s.e.m.). Thus the FRET efficiency ratios and dynamics are not affected markedly by proximity to colloidal particles.

To determine specific codon dependent binding of tRNA in the A site of the ribosomes and the activity of the translocase, elongation factor G, we measured binding of Cy5-Arg-$tRNA^{Arg}$ to Cy3-L11-labeled initiation complexes. In absence of EF-G, Cy5-Arg-$tRNA^{Arg}$ is expected to bind to the A-site of the initiation complex to form the pre-translocation complex with dipeptide fMet-Arg-Cy5-$tRNA^{Arg}$ in the A-site. The Cy5-$tRNA^{Arg}$ is positioned for strong excitation by FRET from Cy3 on the L11. Similar to the tRNA-tRNA FRET described above, two peaks in distributions of FRET efficiency were found. As on plain glass, many ribosomes oscillated back and forth between high and low L11-tRNA FRET efficiency values (assigned to classic and hybrid states), and some of them remained at stable high or low FRET values. The L11-tRNA FRET efficiencies for pre-translocation complexes near silver particles averaged 0.82 and 0.48 with dwell times of 1.84 ± 0.1 s and 0.93 ± 0.05 s in the high and low FRET states, respectively (Fig. 4b-e). These values were similar to high and low FRET values of 0.81 and 0.47 on plain glass with dwell times of 2.0 ± 0.2 s and 0.6 ± 0.04 s, respectively (Fig. 5b-e).

We then checked translocation activity in the pre-complexes with $tRNA^{fMet}$ in the P site and fMet-Arg-Cy5-$tRNA^{Arg}$ in the A site. In 3 fields of 50 x 50 µm each, after addition of 2 µM EF-G and 3 mM GTP, only 36 (8%) particles showed FRET out of 450 colocalized Cy3 and Cy5 molecules near silver colloidal particles similar to 10% of molecules showing FRET on plain glass. This indicates that upon infusion of EF-G into the channel, 92% of fMet-Arg-Cy5-$tRNA^{Arg}$ complexes translocated from the A to the P site of ribosome and thereby lost FRET, which is comparable to the activity of EF-G on plain glass. The disappearance of FRET was not

due to fMet-Arg-Cy5-tRNA^{Arg} dissociation from the ribosome, because alternating laser excitation (ALEX) (46) between 532 nm and 640 nm excitation showed that the Cy3 and Cy5 were still present and colocalized on the ribosomes. Thus the fMet-Arg-Cy5-tRNA^{Arg} translocated and remained in the P site in ribosomes near silver particles.

Figures

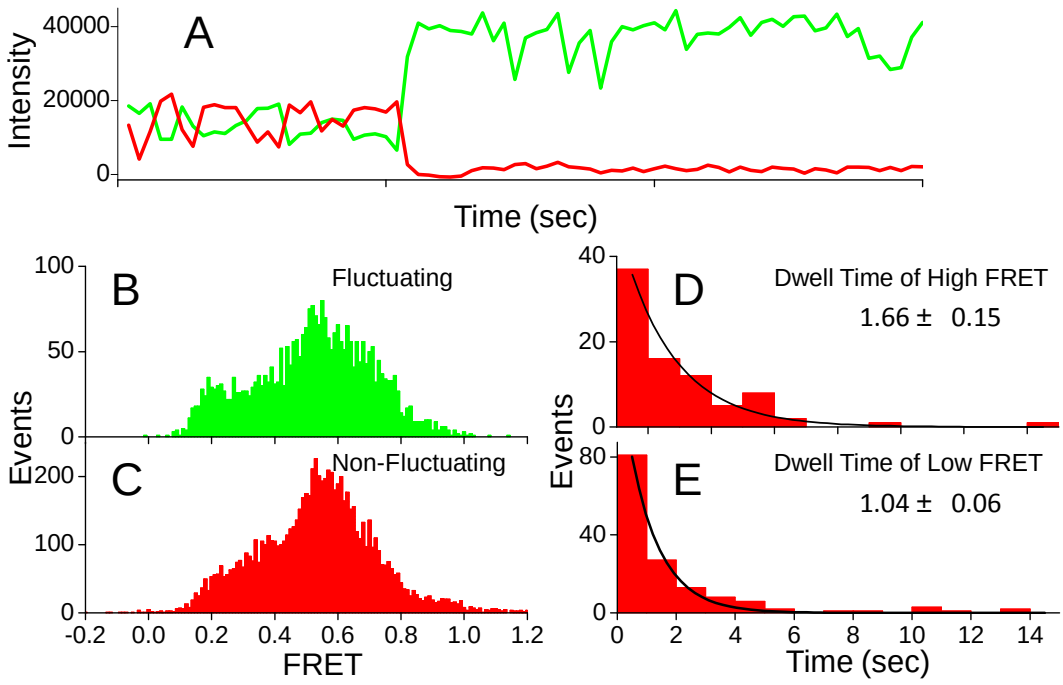

Fig 1 Time courses of fluorescence intensity of pre-complex (PRE-II-tt, having Cy3-tRNA^{Arg} in P site and Cy5-fMet-Arg-Phe-tRNA^{Phe} in the A site) close to silver particles on small silver particle coated glass surface. Cy3 (green) and Cy5 (red) fluorescence intensity traces of PRE-II-tt complex close to silver particles on small silver particles coated glass surface (A) under 532 nm laser illumination. FRET efficiency distributions from fluctuating and non-fluctuating complexes are shown in B and C, respectively. (D) and (E) are dwell time distributions for high and low FRET states, respectively.

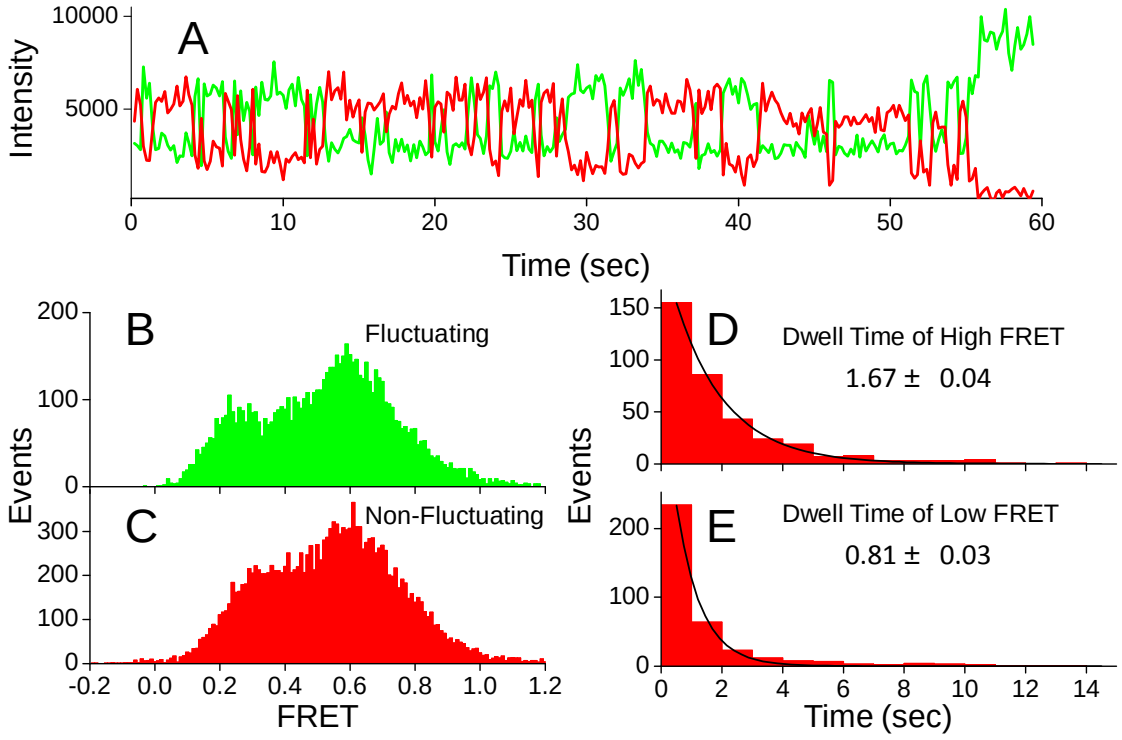

Fig 2 Time courses of fluorescence intensity of pre-complex (PRE-II-tt, having Cy3-tRNA^{Arg} in P site and Cy5-fMet-Arg-Phe-tRNA^{Phe} in the A site) away from silver particles on small silver particle coated glass surface. Cy3 (green) and Cy5 (red) fluorescence intensity traces of PRE-II-tt complex away from silver particles on small silver particles coated glass surface (A) under 532 nm laser illumination. FRET efficiency distributions from fluctuating and non-fluctuating complexes are shown in B and C, respectively. (D) and (E) are dwell time distributions for high and low FRET states, respectively.

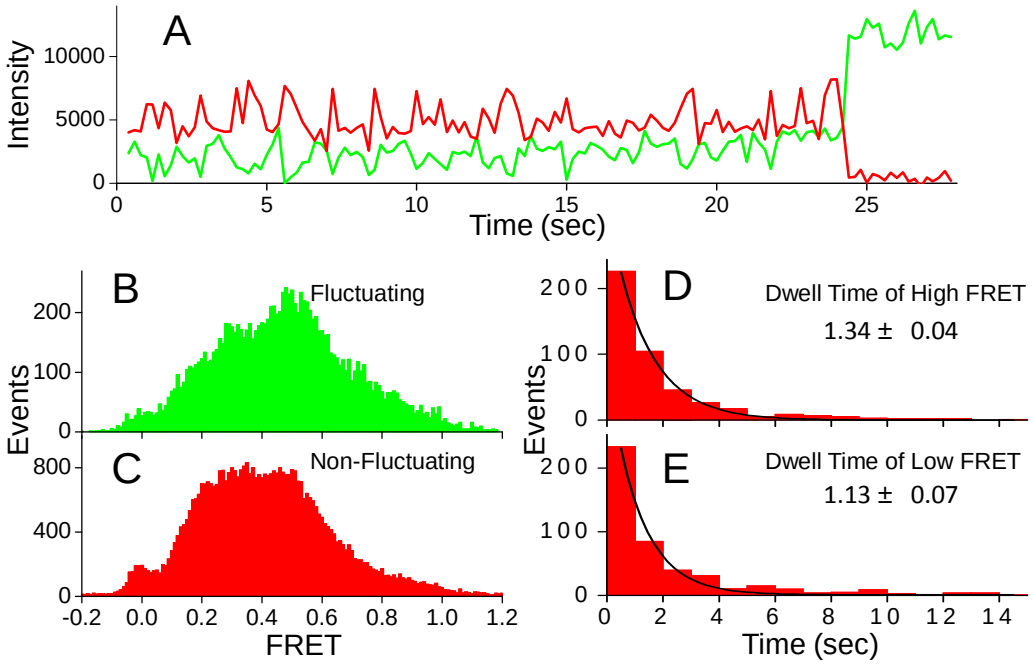

Fig 3 Time courses of fluorescence intensity of pre-complex (PRE-II-tt, having Cy3-tRNA^{Arg} in P site and Cy5-fMet-Arg-Phe-tRNA^{Phe} in the A site) on plain glass. Cy3 (green) and Cy5 (red) fluorescence intensity traces of PRE-II-tt complex on plain glass (A) under 532 nm laser illumination. FRET efficiency distributions from fluctuating and non-fluctuating complexes are shown in B and C, respectively. (D) and (E) are dwell time distributions for high and low FRET states, respectively.

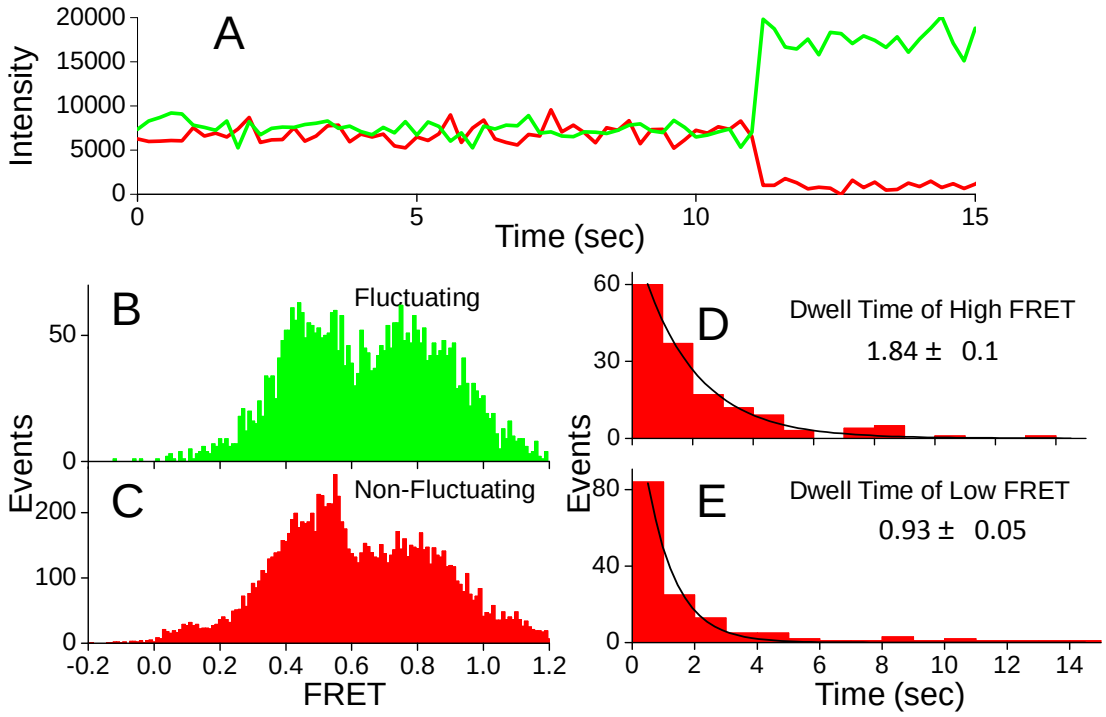

Fig 4 Time courses of fluorescence intensity of pre-complex (PRE-I-Lt, having $tRNA^{fMet}$ in P site and Cy5-fMet-Arg-$tRNA^{Arg}$ in the A site that is labeled with Cy3 at L11 protein) close to silver particles on small silver particle coated glass surface. Cy3 (green) and Cy5 (red) fluorescence intensity traces of PRE-I-Lt complex close to silver particles (A) under 532 nm laser illumination. Similarly, FRET efficiency distributions from fluctuating and non-fluctuating complexes are shown in B and C, respectively. (D) and (E) are dwell time distributions for high and low FRET states, respectively.

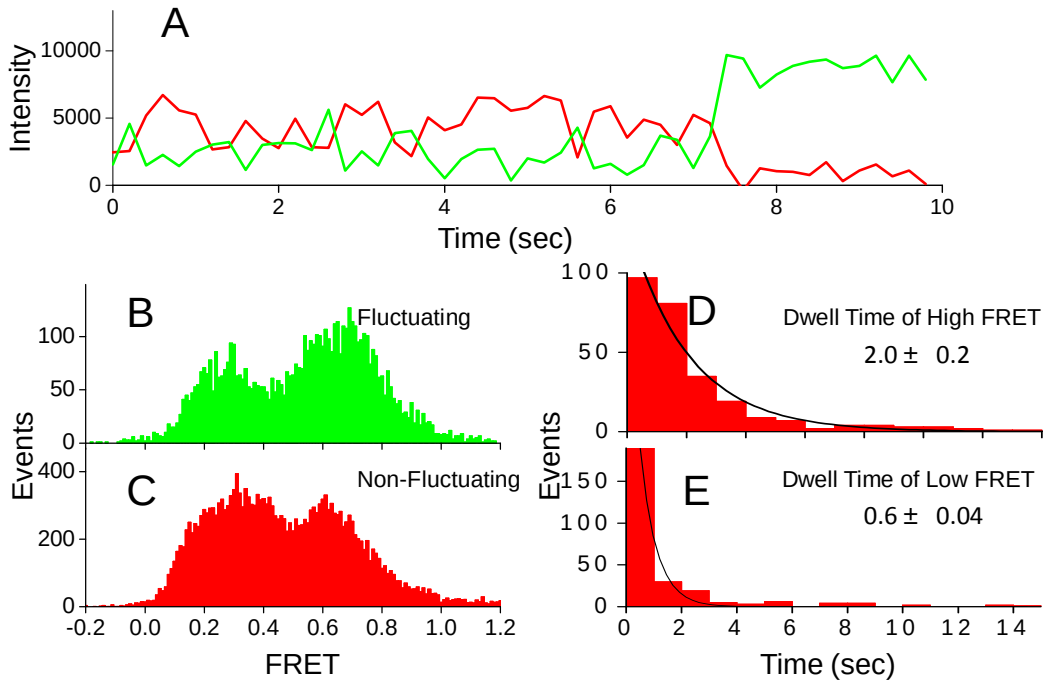

Fig 5 Time courses of fluorescence intensity of pre-complex (PRE-I-Lt, having $tRNA^{fMet}$ in P site and Cy5-fMet-Arg-$tRNA^{Arg}$ in the A site that is labeled with Cy3 at L11 protein) on plain glass. Cy3 (green) and Cy5 (red) fluorescence intensity traces of PRE-I-Lt complex on plain glass (A) under 532 nm laser illumination. Similarly, FRET efficiency distributions from fluctuating and non-fluctuating complexes are shown in B and C, respectively. (D) and (E) are dwell time distributions for high and low FRET states, respectively.

CHAPTER VII

DISCUSSION/CONCLUSION

We here present an application of metal enhanced fluorescence (MEF) for single molecule studies of protein synthesis. Although MEF has previously been shown for many fluorophores, including Cy3 and Cy5, prior to the present work it was unknown whether proximity to colloidal silver particles affects the recording time before photobleaching. Our results clearly show a 4 - 7-fold enhancement of fluorescence intensity of labeled ribosomal initiation complexes (ICs) near silver colloidal particles compared to that seen with PEG over plain glass. Changes in photobleaching rate are minor. The enhancement of fluorescence intensity leads to a 4- and 5-fold increase in total number of photons collected for Cy3 and Cy5 labeled (ICs), respectively. Larger colloids enhance the fluorescence signal more than smaller ones, as expected from earlier reports, (1), but in the size range of 50-85 nm tested here, enhancement of total numbers of photons from Cy5 fluorescence does not depend on the particle size. We found that excess 0.1 – 5 Hz fluctuations of fluorescence intensity from surfaces coated with colloidal silver particles, led to an overall signal to noise ratio either similar to or slightly enhanced relative to fluorescent labeled ICs on plain glass. The recording time before photobleaching under laser illumination is inversely proportional to laser intensity (71). Therefore, we expect that the enhancement can be used effectively to extend the recording time before photobleaching. The lack of MEF effect on photobleaching time is critical for future MEF applications, since a shortened photobleaching time might make MEF an unrealistic approach for

studying lengthy processes such as protein synthesis. Our work also represents the first application of MEF to the study of a supramolecular complex, in this case the ribosome. The similarities in the results obtained for pretranslocation and posttranslocation complexes bound near silver colloidal particles compared to those bound to plain glass strongly suggest that MEF did not significantly compromise the activity of initiation complexes, binding to the ribosome of cognate aminoacyl-tRNAs via ternary complexes, or translocation catalyzed by EF-G.

Ribosomes bound randomly to the surface, either near or far from the colloids. In principle, virtually all of the labeled ribosomes that co-localize with the silver particles should give MEF, while all those that do not co-localize should not. In practice we found that 70 - 80% of the co-localized labeled ribosomes had high intensity, as compared with 20-30% of the non-colocalized ribosomes. The higher than expected intensities for some of the non-localized ribosomes (non-colocalized spots, Fig. S4A) are most likely attributable to incomplete identification of the colloidal particles by light scattering due to the noise and limited sensitivity of the camera. This explanation is supported by the very small number of high intensity spots found on plain glass and that a 3 - 4-fold higher density of particles was detected by AFM than by light scattering. The lower than expected intensities for some of the co-localized ribosomes most likely reflects limited resolution of co-localization (~250 nm), as well as quenching of fluorescence, which is expected when fluorophores are within 2 nm of colloids (72). The latter effect should be quite limited, however, since the 5,000 Da PEG coating the surface was approximately 5 nm thick. In addition the mRNA strand linking the ribosome to the PEG was ~5 nm long. The estimate of the radius surrounding the colloidal particles that provided fluorescence enhancement, according to the density of particles and the proportion of enhanced fluorophores, ~270 nm, would also need to be adjusted if a central region is quenched, rather than enhanced.

Another major issue in the use of MEF is long wavelength luminescence from bare colloids that overlaps the emission spectra of the fluorophores, thereby potentially interfering with single molecule measurements. This concern led us to characterize the luminescence signal of the colloids. We verified that silver particles give rise to luminescence, and investigated why some of the particles were much brighter than others. According to the resonant extinction theory (65-67), when two colloidal particles are closer to each other than their diameters, resonant scattering and absorption causes loss of energy and scattering at longer wavelength. As a result, the spectral properties of the emission should depend on the size of the particles and their state of aggregation. For a given spectral detection band, a minimum size would be required to observe resonant emission, so that the intensity and emission wavelength from colloids would be correlated with their sizes. We, indeed, found these relations to hold (Fig. 3 and Table S1), with smaller colloids showing fewer luminescing particles with lower intensity. For the smFRET results reported in this study, we selected molecules that showed only single step photobleaching to a stable background to distinguish fluorescence emission of Cy3 and Cy5 from colloidal luminescence. In contrast, the luminescence signal from colloidal aggregates either does not bleach or bleaches slowly and gradually, and never in a single step. In conclusion, this study shows that metal enhanced fluorescence with 50-85 nm silver colloidal particles could be successfully applied in studies of biological processes involving supramolecular complexes. We found that ribosomal complexes are fully active near these particles. We observed long wavelength luminescence background and excess noise associated with many of the silver particles. The background could be eliminated as a problem by using single step photobleaching to select organic fluorophores. These results engender confidence that metal enhanced

fluorescence will be useful in further studies of ribosomes, and quite possibly, of many other types of supramolecular complexes.

REFERENCES

(1) Lakowicz, J. R. *Principles of Fluorescence Spectroscopy* (Kluwer Academic/Plenum Publishers, New York, 2006).

(2) Mason, W. *A Practical Guide to Technology for Quantitative Real-Time Analysis: Fluorescent and Luminescent Probes for Biological Activity* (Academic Press, New York, 1999).

(3) Lukas, T. J., Burgess, W. H., Prendergast, F. G., Lau, W., Watterson, D. M. Calmodulin binding domains: characterization of a phosphorylation and calmodulin binding site from myosin light chain kinase.. *Biochemistry* **25**, 1458-1464 (1986).

(4) LeTilly, V., Royer, C. A. Fluorescence anisotropy assays implicate protein-protein interactions in regulating trp repressor DNA binding**.** *Biochemistry* **32**, 7753-7758 (1993).

(5) Pack, C. G., Nishimura, G., Tamura, M., Aoki, K., Taguchi, H., Yoshida, M., Kinjo, M. Analysis of interaction between chaperonin GroEL and its substrate using fluorescence correlation spectroscopy. *Cytometry* **36**, 247-253 (1999).

(6) Kahya, N., Scherfeld, D., Bacia, K., Poolman, B., Schwille, P. Probing lipid mobility of raft-exhibiting model membranes by fluorescence correlation spectroscopy. *J. Biol Chem.* **278**, 28109-28115 (2003).

(7) Lakowicz, J. R., Gryczynski, I., Wiczk, W., Laczko, G., Prendergast, F. C., Johnson, M. L. Conformational distributions of melittin in water/methanol mixtures from frequency-domain measurements of nonradiative energy transfer. *Biophys Chem.* **36**, 99-115 (1990).

(8) Xu Q, Brecht WJ, Weisgraber KH, Mahley RW, Huang Y. Apolipoprotein E4 domain interaction occurs in living neuronal cells as determined by fluorescence resonance energy transfer. *J. Biol Chem.* **279**, 25511-25516 (2004).

(9) Kapanidis, A. N., Strick, T. Biology, one molecule at a time. *Trends Biochem Sci*. **34**, 234-243 (2009).

(10) Alemán, E. A., Lamichhane, R., Rueda, D. Exploring RNA folding one molecule at a time. *Curr Opin Chem Biol.* **12**, 647-654 (2008).

(11) Deniz, A. A., Mukhopadhyay, S., Lemke, E. A. Single-molecule biophysics: at the interface of biology, physics and chemistry. *J R Soc Interface* **5**, 15-45 (2008).

(12) Peters, R. Single-molecule fluorescence analysis of cellular nanomachinery components. *Annu Rev Biophys Biomol Struct.* **36**, 371-394 (2007).

(13) Bustamante, C., Bryant, Z., Smith, S. B. Ten years of tension: single-molecule DNA mechanics. *Nature* **421**, 423-427 (2003).

(14) Roy, R., Hohng, S., Ha, T. A practical guide to single-molecule FRET. Nat Methods **5**, 507-516 (2008).

(15) Kapanidis, A. N., Laurence, T. A., Lee, N. K., Margeat, E., Kong, X., Weiss, S. Alternating-laser excitation of single molecules. *Acc Chem Res*. **38**, 523-533, (2005).

(16) Shimon, W. Fluorescence spectroscopy of single biomolecules. *Science* **283**, 1676-1683, (1999).

(17) Gell, C., Brockwell, D., Smith, A. *Handbook of Single Molecule Fluorescence Spectroscopy: Preparation of Samples for Single Molecule Fluorescence Spectroscopy* Ch. 4 (Oxford Univ. Press, Oxford, 2006).

(18) Lee, S. F., Osborne, M. A., Brightening, blinking, bluing and bleaching in the life of a quantum dot: friend or foe?. *Chemphyschem*. **10**, 2174-91, (2009).

(19) Aslan, K., Gryczynski, I., Malicka, J., Matveeva, E., Lakowicz, J. R., Geddes, C.D. Metal-enhanced fluorescence: an emerging tool in biotechnology. *Curr Opin Biotechnol*. **16**, 55-62, (2005).

(20) Lakowicz, J. R., Radiative decay engineering 5: metal-enhanced fluorescence and plasmon emission. *Anal. Biochem*. **337**, 171-194, (2005).

(21) Lakowicz, J. R., Radiative decay engineering: biophysical and biomedical applications. *Anal. Biochem*. **298**, 1-24, (2001).

(22) Ghosh, S. K., Pal, T. Interparticle coupling effect on the surface plasmon resonance of gold nanoparticles: from theory to applications. *Chem. Rev.* **107**, 4797-4862, (2007).

(23) Malicka, J., Gryczynski, I., Fang, J., Lakowicz, J. R. Fluorescence spectral properties of cyanine dye-labeled DNA oligomers on surfaces coated with silver particles. *Anal Biochem.* **317**, 136-146 (2003).

(24) Fu, Y., Lakowicz, J. R. Single-molecule studies of enhanced fluorescence on silver island films. *Plasmonics* **2**, 1-4, (2007).

(25) Mathews, C. K., Van Holde, K. E., Ahern, K. G. *Biochemistry: Information Decoding: Translation* Ch. 27 (Addison Wesley Longman, San Francisco, 2000).

(26) Stryer, L. *Biochemistry: Protein Synthesis* Ch. 34 (W. H. Freeman and Company, NY, 1995).

(27) Ross, J. mRNA stability in mammalian cells. *Microbiol Rev.* **59**, 423-50 (1995).

(28) Ramakrishnan, V. Ribosome structure and the mechanism of translation. *Cell* **108,** 557-572 (2002).

(28a) Yusupov, M. M., Yusupova, G. Z., Baucom, A., Lieberman, K., Earnest, T. N., Cate, J. H., Noller, H. F. Crystal structure of the ribosome at 5.5 A˚ resolution. *Science* **292**, 883–896 (2001).

(29) Ban, N., Nissen, P., Hansen, J., Moore, P. B., Steitz, T. A. The complete atomic structure of the large ribosomal subunit at 2.4 A° resolution. *Science* **289**, 905–920 (2000).

(30) Harms, J., Schluenzen, F., Zarivach, R., Bashan, A., Gat, S., Agmon, I., Bartels, H., Franceschi, F., Yonath, A. High resolution structure of the large ribosomal subunit from a mesophilic eubacterium. *Cell* **107**, 679–688 (2001).

(31) Schluenzen, F., Tocilj, A., Zarivach, R., Harms, J., Gluehmann, M., Janell, D., Bashan, A., Bartels, H., Agmon, I., Franceschi, F., Yonath, A. Structure of functionally activated small ribosomal subunit at 3.3 A° resolution. *Cell* **102**, 615–623 (2000).

(32) Wimberly, B. T., Brodersen, D. E., Clemons, W. M., Morgan-Warren, R. J., Carter, A. P., Vonrhein, C., Hartsch, T., Ramakrishnan, V. Structure of the 30S ribosomal subunit. *Nature* **407**, 327–339 (2000).

(33) Schlunzen, F., Zarivach, R., Harms, J., Bashan, A., Tocilj, A., Albrecht, R., Yonath, A., Franceschi, F. Structural basis for the interaction of antibiotics with the peptidyl transferase centre in eubacteria. *Nature* **413**, 814–821 (2001).

(34) Yusupov, M. M., Yusupova, G. Z., Baucom, A., Lieberman, K., Earnest, T. N., Cate, J. H., Noller, H. F. Crystal structure of the ribosome at 5.5 A˚ resolution. *Science* **292**, 883–896 (2001).

(35) Hartz, D., Binkley, J., Hollingsworth, T., and Gold, L. Domains of initiator tRNA and initiation codon crucial for initiator tRNA selection by *Escherichia coli* IF3. *Genes Dev*. **4**, 1790–1800 (1990).

(36) Ogle, J. M., Brodersen, D. E., Clemons, W. M., Jr., Tarry, M. J., Carter, A. P., Ramakrishnan, V. Recognition of cognate transfer RNA by the 30S ribosomal subunit. *Science* **292**, 897–902 (2001).

(37) Nierhaus, K. H., Schulze, H., Cooperman, B. S. Molecular mechanisms of the ribosomal peptidyltransferase center. *Biochem. Int*. **1**, 185–192 (1980).

(38) Nissen, P., Hansen, J., Ban, N., Moore, P. B., and Steitz, T. A. The structural basis of ribosome activity in peptide bond synthesis. *Science* **289**, 920–930 (2000).

(39) Thompson, J., Kim, D. F., O'Connor, M., Lieberman, K. R., Bayfield, M. A., Gregory, S. T., Green, R., Noller, H. F., and Dahlberg, A. E. Analysis of mutations at residues A2451 and G2447 of 23S rRNA in the peptidyltransferase active site of the 50S ribosomal subunit. *Proc. Natl. Acad. Sci. USA* **98**, 9002–9007 (2001).

(40) Bretscher, M. S. Translocation in protein synthesis: a hybrid structure model. *Nature* **218**, 675–677 (1968).

(41) Moazed, D., and Noller, H. F. Intermediate states in the movement of transfer RNA in the ribosome. *Nature* **342**, 142–148 (1989).

(42) Lukomska, J., Gryczynski, I., Malicka, J., Makowiec, S., Lakowicz, J. R., Gryczynski, Z. One- and two-photon induced fluorescence of pacific blue-labeled human serum albumin deposited on different core size silver colloids. *Biopolymers* **81**, 249-255 (2005).

(43) Seo, H. S., Abedin, S., Kamp, D., Wilson, D. N., Nierhaus, K. H., Cooperman, B. S. EF-G-dependent GTPase on the ribosome. conformational change and fusidic acid inhibition. *Biochemistry* **45**, 2504-2514 (2006).

(44). Wang, Y., Qin, H., Kudaravalli, R. D., Kirillov, S. V., Dempsey, G. T., Pan, D., Cooperman, B. S., Goldman, Y. E. Single-molecule structural dynamics of EF-G-ribosome interaction during translocation. *Biochemistry* 46, 10767-1075 (2007).

(45) Pan, D., Qin, H., Cooperman, B. S. Synthesis and functional activity of tRNAs labeled with fluorescent hydrazides in the D-loop. *RNA* **15**, 346-354 (2009).

(46) Kapanidis, A. N., Laurence, T. A., Lee, N. K., Margeat, E., Kong, X., Weiss, S. Alternating-laser excitation of single molecules. *Acc Chem Res*. **38**, 523-533, (2005).

(47) Sabanayagam, C. R., Eid, J. S., Meller, A. High-throughput scanning confocal microscope for single molecule analysis. Appl Phys Lett. **84**, 1216-1218 (2004).

(48) Ha, T. J., Ting, A. Y., Liang, J., Caldwell, W. B., Deniz, A. A., Chemla, D. S., Schultz, P. G., Weiss, S., Single-molecule fluorescence spectroscopy of enzyme conformational dynamics and cleavage mechanism. *Proc Natl Acad Sci USA* **96**, 893-898 (1999).

(49) McKinney, S. A., Joo, C., Ha, T. Analysis of single-molecule FRET trajectories using hidden Markov modeling. *Biophys J.*, **91**, 1941-1951 (2006).

(50) Peterman, E. J. G., Sosa, H., Moerner, W. E. Single-molecule fluorescence spectroscopy and microscopy of biomolecular motors. *Annu. Rev. Phys. Chem.* **55**, 79–96 (2004).

(51) Yanagida, T., Ishii, Y. *Single Molecule Dynamics in Life Sciences: Imaging and Molecular Motors* Ch. 3 (Wiley-VCH, Weinheim, 2009).

(52) Ross, J. L., Wallace, K., Shuman, H., Goldman, Y. E., Holzbaur, E. L. Processive bidirectional motion of dynein-dynactin complexes *in vitro*. *Nat Cell Biol*. **8**, 562-570 (2006).

(53) Sun, Y., Schroeder, H. W. 3rd, Beausang, J. F., Homma, K., Ikebe, M., Goldman, Y. E. Myosin VI walks "wiggly" on actin with large and variable tilting. *Mol Cell*. 28, 954-964 (2007).

(54) Dixit, R., Ross, J. L., Goldman, Y. E., Holzbaur, E. L. Differential regulation of dynein and kinesin motor proteins by tau. *Science* 22, 1086-1089 (2008).

(55) Galburt, E. A., Grill, S. W., Bustamante, C. Single molecule transcription elongation. *Methods* **48**, 323-332 (2009).

(56) Davenport, R. J., Wuite, G. J., Landick, R., Bustamante C. Single-molecule study of transcriptional pausing and arrest by E. coli RNA polymerase. *Science* **287**, 2497–2500 (2000).

(57) Blanchard, S. C. Single-molecule observations of ribosome function. *Curr Opin Struct Biol.* **19**, 103-109 (2009).

(58) Vanzi, F., Takagi, Y., Shuman. H, Cooperman, B. S., Goldman, Y. E. Mechanical studies of single ribosome/mRNA complexes. *Biophys J*. **89**, 1909-1919 (2005).

(59) Resch-Genger, U., Grabolle, M., Cavaliere-Jaricot, S., Nitschke, R., Nann, T. Quantum dots versus organic dyes as fluorescent labels. *Nature methods*, 5, 763-775 (2008).

(60) Shaner, N. C., Steinbach, P. A., Tsien, R. Y. A guide to choosing fluorescent proteins. *Nature Methods* **2**, 905-909 (2005).

(61) Miyawaki, A., Sawano, A., Kogure, T. Lighting up cells: labeling proteins with fluorophores. *Nat Cell Biol*., Suppl:S1-7 (2003).

(62) Wilhelm, J. M., Haselkorn, R. The chain growth rate of T4 lysozyme *in vitro*. *Proc Natl Acad Sci USA* **65**, 388-394 (1970).

(63) Young, R., Bremer, H. Polypeptide-chain-elongation rate in Escherichia coli B/r as a function of growth rate. *Biochem J*. **160**, 185-194 (1976).

(64) Govorov, A. O., Carmeli, I. Hybrid structures composed of photosynthetic system and metal nanoparticles: plasmon enhancement effect. *Nano lett.* **7**, 620-625 **(**2007).

(65) Yguerabide, J., Yguerabide, E. E., Light-scattering submicroscopic particles as highly fluorescent analogs and their use as tracer labels in clinical and biological applications. *Anal Biochem.* **262**, 137-156 (1998).

(66) Quinten, M., Kreibig, U. Absorption and elastic scattering of light by particle aggregates. *Appl Opt*. **32**, 6173-6182 (1993).

(67) Kreibig, U. *Optical Properties of Metal Clusters* (Springer, New York, 1994).

(68) Bike, S. G. Measuring colloidal forces using evanescent wave scattering, *Curr. Opin. Colloid Interface Sci.* **5**, 144-150 (2000).

(69) Munro, J. B., Altman, R. B., O'Connor, N., Blanchard, S. C. Identification of two distinct hybrid state intermediates on the ribosome. *Mol Cell*. **25**, 505-517 (2007).

(70) Blanchard, S. C., Kim, H. D., Gonzalez, R. L. Jr., Puglisi, J. D., Chu, S. tRNA dynamics on the ribosome during translation. *Proc Natl Acad Sci USA* **101**, 12893-12898 (2004).

(71) Quinlan, M. E., Forkey, J. N., Goldman, Y. E. Orientation of the myosin light chain region by single molecule total internal reflection fluorescence polarization microscopy. *Biophys J*. **89**, 1132-42 (2005).

(72) Malicka, J., Gryczynski, I., Gryczynski, Z., Lakowicz, J. R. Effects of fluorophore-to-silver distance on the emission of cyanine–dye-labeled oligonucleotides. *Anal Biochem.* **315**, 57-66 (2003).

PUBLICATIONS

1. Shashank Bharill, Chunlai Chen, Benjamin Stevens, Jaskiran Kaur, Zeev Smilansky, Wlodek Mandecki, Ignacy Gryczynski, Zygmunt Gryczynski, Barry S. Cooperman and Yale E. Goldman (2010). Enhancement of Single Molecule Fluorescence Signals by Colloidal Silver Nanoparticles in Studies of Ribosome Dynamics. ***Nature Nanotechnology*****, Submitted and Under Review,**

2. Ignacy Gryczynski, Luchowski, **Shashank Bharill**, Julian (2009). Ch.12, Non-linear Curve Fitting Methods for Time-Resolved Data Analysis. ***FLIM Microscopy in Biology and Medicine*** *by Ammasi Periasamy and Robert M. Clegg* , ,

3. Teresa Duda, **Shashank Bharill**, Prem, Ignacy Gryczynski, Zygmunt Gryczynski and Rameshwar Sharma (2009). Atrial natriuretic factor receptor guanylate cyclase signaling: new ATP-regulated transduction motif. ***Mol Cell Biochem*****, 324, 39-53**

4. Roberto Ramoni, Maria Staiano, Stefano Bellucci, Ignacy Grycznyski, Zygmunt Grycznyski, Roberta Crescenzo, Luisa Iozzino, **Shashank Bharill**, Virna Conti, Stefano Grolli and Sabato D'Auria (2008). Carbon nanotube-based biosensors. ***J. Phys.: Condens. Matter*****, 20, 474201**

5. Rafal Luchowski, Pabak Sarkar, **Shashank Bharill**, Gabor Laczko, Julian Borejdo, Zygmunt Gryczynski, and Ignacy Gryczynski (2008). Fluorescence polarization standard for near infra red spectroscopy and microscopy. ***Applied Optics*****, 33, 6257-65**

6. I. Gryczynski , E.G. Matveeva , P. Sarkar , **S. Bharill** , J. Borejdo, W. Mandecki , I. Akopova ,

Z. Gryczynski (2008). Metal enhanced fluorescence on silicon wafer substrates. ***Chemical Physics Letters*****, 462, 327-330**

7. Pabak Sarkar, **Shashank Bharill**, Ignacy Gryczynski, Zygmunt Gryczynski, Maya P. Nair and Andras G. Lacko (2008). Binding of 8-Anilino-1- Naphtalenesulfonate to Lecitin: Cholesterol Acyltransferase Studied by Fluorescence Techniques. ***Journal of Photochemistry and Photobiology*****, 92, 19-23**

8. Ballin JD, Prevas JP, **Bharill S**, Gryczynski I, Gryczynski Z, Wilson GM (2008). Local RNA conformational dynamics revealed by 2-aminopurine solvent accessibility. ***Biochemistry,*** **47, 7043-52**

9. Shashank Bharill, Pabak Sarkar, Jeff Balin, Ignacy Gryczynski, Gerald Wilson and Zygmunt Gryczynski (2008). Fluorescence Intensity Decays of 2-Aminopurine solutions: Lifetime Distribution Approach. ***Analytical Biochemistry*****, 377, 141-9**

10. Wlodek Mandecki; **Shashank Bharill**; Julian Borejdo; Diana Cabral; Barry S. Cooperman; Ian Farrell; Linus Fetter; Emanuel Goldman; Zygmunt Gryczynski; Hieronim Jakubowski; Hanqing Liu; Rafal Luchowski; Evgenia Matveeva; Dongli Pan; Haiou Qin; Donald Tennan (2008). Fluorescence enhancement on silver nanostructures studies of components of ribosomal translation in vitro. ***Proc SPIE*****, 6862,**

11. Jeff D. Ballin, **Shashank Bharill**, Elizabeth J. Fialcowitz-White, Ignacy Gryczynski,

Zygmunt Gryczynski, and Gerald M. Wilson (2007). Site-Specific Variations in RNA Folding Thermodynamics Visualized by 2-Aminopurine Fluorescence. ***Biochemistry*, 46, 13948-60**

12. Piotr Bojarski, Ignacy Gryczyski, Leszek Kuak, Anna Synak, **Shashank Bharill**, Simeonika Rangeowa and Mariusz Szabelski (2007). Multistep energy migration between 3,3-diethyl-9-methylthiacarbocyanine iodide monomers in uniaxially oriented polymer films. ***Chemical Physics Letters*, 439, 332-36**

13. Hanna Grajek, Ignacy Gryczynski, Piotr Bojarski, Zygmunt Gryczynski, **Shashank Bharill** and Leszek Kuak (2007). Flavin mononucleotide fluorescence intensity decay in concentrated aqueous solutions. ***Chemical Physics Letters*, 439, 151-156**

14. Z. Gryczynski; I. Gryczynski; E. G. Matveeva; N. Calander; R Grygorczyk; I. Akopova; **S. Bharill;** P. Muthu; S. Klidgar; J. Borejdo (2007). New surface plasmons approach to single molecule detection (SMD) and fluorescence correlation spectroscopy (FCS). ***Proc SPIE*, 6444,**